Highlights

- An efficient NUBRS-based formulation is proposed to deal with the size effects of small-scale functionally graded plates.
- A novel seventh-order quasi-3D plate theory with only four unknowns requiring C^1-continuity is used to sufficiently describe the shear deformation and stretching effects through plate's thickness.
- A modified couple stress theory with only one material length scale parameter, which requires second-order derivatives of the unknowns, efficiently captures the size effects of the microplates.
- The reliability and validity of the proposed method are illustrated by a number of convergence and comparison results including benchmark numerical examples.
- Effects of material length scale parameter, material index and plate's aspect ratio on the mechanical behaviours of microplates are investigated.

A Refined Quasi-3D Isogeometric Analysis for Functionally Graded Microplates based on the Modified Couple Stress Theory

Hoang X. Nguyen[a], Tuan N. Nguyen[b], M. Abdel-Wahab[c], S.P.A. Bordas[d], H. Nguyen-Xuan[e,f,*], Thuc P. Vo[a,*]

[a]*Department of Mechanical and Construction Engineering, Northumbria University, Newcastle upon Tyne NE1 8ST, United Kingdom*

[b]*Department of Computational Engineering, Vietnamese-German University, Binh Duong New City, Vietnam*

[c]*Laboratory Soete, Faculty of Engineering and Architecture, Ghent University, 9000 Ghent, Belgium*

[d]*Faculté des Sciences, de la Technologie et de la Communication, University of Luxembourg, Luxembourg*

[e]*Department of Physical Therapy, Graduate Institute of Rehabilitation Science, China Medical University, Taichung 40402, Taiwan*

[f]*Center for Interdisciplinary Research in Technology (CIRTech), Ho Chi Minh University of Technology (HUTECH), Ho Chi Minh City 700000, Vietnam*

Abstract

The isogeometric analysis associated with a novel quasi-3D shear deformation theory is proposed to investigate size-dependent behaviours of functionally graded microplates. The modified couple stress theory with only one material length scale parameter is employed to effectively capture the size-dependent effects within the microplates. Meanwhile, the quasi-3D theory which is constructed from a novel seventh-order shear deformation refined plate theory with four unknowns is able to consider both shear deformations and thickness stretching effect without requiring shear correction factors. The NURBS-based isogeometric analysis is integrated to exactly describe the geometry and approximately calculate the unknown fields with higher-order derivative and continuity requirements. The proposed approach is successfully applied to study the static bending, free vibration and buckling responses of rectangular and circular functionally graded microplates with various types of boundary conditions in which some benchmark numerical examples are presented. A number of investigations are also conducted to illustrate the effects of the material length scale, material index, and aspect ratios on the responses of the microplates.

Keywords: Isogeometric analysis, Functionally graded microplates, Modified couple stress theory, Refined plate theory, Quasi-3D theory.

*Corresponding author

Email addresses: xuan.h.nguyen@northumbria.ac.uk (Hoang X. Nguyen), ngx.hung@hutech.edu.vn (H. Nguyen-Xuan), thuc.vo@northumbria.ac.uk (Thuc P. Vo)

1. Introduction

Functionally graded materials (FGMs) are composite materials formed of two or more constituent phases in which material properties vary smoothly within the structure. Consequently, FGMs avoid high interlaminar shear stresses, stress concentration and delamination phenomena which are often cited as shortcomings of laminated composite materials. A FGM consisting of ceramic and metal possesses higher thermal resistance and better ductility which are inherited from the ceramic and metal phases, respectively. Owing to these striking features, FGMs are applicable to various fields of engineering including aerospace, nuclear power, chemistry and bio-engineering. FGMs have also been widely studied for various types of structures such as beams [1–4], plates [5–8], and shells [9–11].

Recent advances in technology lead to new industrial fields in which small-scale elements are involved. Such elements have been applied in micro- and nano-electro-mechanical systems [12, 13], actuators [14], space and bio-engineering [15]. These applications encourage new research area that focuses on investigating and predicting the behaviours of such micro structures. A number of approaches have been employed to analyse the characteristics of small-scale structures both experimentally and numerically [16, 17]. Indeed, typical structural sizes range from a few to dozens of polycrystalline grains only, such that the actual local grain morphology has a strong influence on the global structural behaviour [18]. One approach is to handle grains explicitly and represent each of them in the model. This leads to large computational demands because of the lack of scale separation. Such constitutive models must be able to account for size effects which are characteristic of small-scale structures. This is confirmed following a number of theoretical and experimental studies of Fleck et al. [19], Stolken and Evans [20], and Lam et al. [21]. From an experimental observation from bending test of epoxy polymeric microbeams, Lam et al. [21] point out that the bending rigidity increases 2.4 times as a result of the reduction of the beam thickness from 115 μm to 20 μm.

In order to take into account the size effects, a number theories have been developed including nonlocal elasticity theory [22], strain gradient theory [23], and modified couple stress theory [24]. It is worth noting that the classical elasticity is fundamentally founded by the introduction of the Hooke's Law in which the force and the change in displacement are linearly related via the stiffness of the component where the forces are applied. This physical principle governs the linearly elastic behaviour of materials. Aiming at a more general description of materials' responses, Mindlin and Tiersten [25] and Mindlin [26] developed higher-order theories of elasticity. Based on the employment of deformation metrics, those theories can be classified into two categories: strain gradient and couple stress theories. With regard to the strain gradient theories, this concept was first developed by Fleck and Hutchinson [23] in which Mindlin's theory [26] was extended. There are two components, which are classified using the second-order deformation tensor that include stretch gradient tensor and rotation gradient tensor [27]. Within the concept of couple stress theory, both strain and curvature jointly govern the strength of the solid. In addition, while the antisymmetric part of the second-order deformation gradients represent rotation gradients, the symmetric part is neglected. Based on the initial ideas of the couple stress theory, a number of attempts

have been conducted to further develop such concepts that are applicable to size-dependent problems. Yang et al. [24] proposed the equilibrium of moment of couples which was an additional equilibrium relation that forces the couple stress tensor to be symmetric. Therefore, the deformation energy is only influenced by the symmetric part of the rotation gradient and the symmetric part of the displacement gradient. In addition, instead of using two material length scale parameters as needed in the classical couple stress theory, this modified couple stress theory (MCST) requires only one material length scale parameter to construct the constitutive relation. Park and Gao [28] utilised the principle of minimum total potential energy to develop a variational formulation of the MCST. This method not only derives the equilibrium equations but also forms the introduction of boundary conditions which are not available in Yang's theory [24]. Possessing those beneficial characteristics in which a symmetric couple stress included and only one material length scale parameter involved, the MCST is considered to have advantages over other size-dependent theories such as classical couple stress theory and nonlocal theory.

In recent years, the MCST has been applied to study various behaviours at small-scales. For beam analysis, static bending, buckling, and vibration analysis have been solved using Euler-Bernoulli [29], Timoshenko [30–33], and higher-order beam theories [34]. The MCST was also applied to small-scale plate analyses in several ways, Tsiatas [35] initially employed it to investigate the static bending response of isotropic Kirchhoff microplates. Yin et al. [36] investigated the vibration behaviour of Kirchhoff microplates using the standard separation of variables to derive the closed-form solution for natural frequencies. Bending and vibration behaviours of Mindlin microplates were studied by Ma et al. [37] in which the thickness stretching effect was also taken into account. With regard to small-scale functionally graded (FG) structures, a number of investigations have been conducted for FG microbeams and microplates using the MCST. Static bending and buckling of FG microbeams were studied by Simsek et al. [38] and Nateghi et al. [39]. Thai and his colleagues utilised the Navier's approach to deriving solutions for FG microplates in which Kirchhoff, Mindlin and sinusoidal plate theories were used [40–42]. Ke et al. [43, 44] employed the p-version of the Ritz method and different quadrature method to solve free vibration and bending, buckling problems of the rectangular and annular FG Mindlin microplates, respectively. Using the MCST, a refined plate theory was utilised to predict the bending, buckling, and vibration behaviours of FG microplates by He et al. [45] following the Navier approach. Reddy et al. [46–49] studied the nonlinear behaviour of small-scale FG microplates for different geometries based on finite element method (FEM) with eleven-unknown C^0 element formulation. Most of these efforts followed either analytical approaches being able to solve specific problem for a limit set of boundary conditions or C^0 FEMs with high number of unknowns which are computationally expensive.

A large proportion of the studies in small-scale FG structures employs the classical plate theory (CPT) and the first-order shear deformation theory (FSDT). However, the CPT (or the Kirchhoff-Love theory), which neglects shear deformation, provides acceptable solutions for thin plates (i.e. length-to-thickness ratios are larger than 20) only. The FSDT (or Reissner-Mindlin plate theory), which accounts for transverse shear effects, is applicable for both thin and moderately thick plates [50–52]. The shortcomings of the FSDT include inac-

curate distribution of transverse shear strain/stress and violation of traction free boundary conditions at the top and bottom surfaces. For this reason, shear correction factors are required to adjust the transverse shear stress distribution. However, these factors vary from problem to problem and one may find it difficult to choose appropriate values in general. In order to avoid using shear correction factors, the third-order shear deformation theory (TSDT) [53], higher-order shear deformation theory (HSDT) [54], sinusoidal shear deformation theory (SSDT) [55], and refined plate theories (RPT) [56] have been developed yielding more accurate and robust results. The RPT was initially proposed by Senthilnathan et al. [56] by employing four independent unknowns which is one less than that of TSDT. Shimpi et al. [57–59] then further developed the RPT for isotropic and orthotropic plates by using only two variables. However, HSDT and RPT require the C^1-continuity of the generalised displacements which cause significant challenge to derive the second derivative of deflection in the framework of finite element analysis (FEA) with C^0 elements. In order to overcome these continuity issues, some C^0 approximations [60] and Hermite interpolation functions with C^1 elements [8] which involve adding extra variables of derivative of displacement can be adopted.

Recently, a new numerical method so-called Isogeometric Analysis (IGA) which is able to deal with C^1-continuity problem without using any additional variables or Hermite interpolation function has been introduced by Hughes and his co-workers [61]. This method bridges the existing gap between computer-aided design (CAD) and the fields of FEA. The essential idea of the IGA is that the basis functions, commonly the non-uniform rational B-splines (NURBS), which are employed to exactly describe the geometry domain will also be used for approximations of the unknown fields. In addition, these basic functions are high smoothness and able to tailor the continuity order easily through the domain [61, 62]. With these striking features, the NURBS-based IGA appears to be a potential approach in dealing with the C^1 HSDT and RPT problems [63]. One may find the guidance on computer implementation of IGA in the literature [64–66]. IGA has been widely implemented in a number of linearly and non-linearly mechanical and thermal problems such as static, free vibration, and buckling of laminated composite and FG plates with various plate theories including layerwise [67], FSDT [68–70], HSDT [71–73], and RPT [63]. The IGA is also applicable for the analysis of the shell structures [74–76]. However, as far as authors are aware, there is no work published on the analysis of small-scale plates based on the MCST and NURBS basis functions.

In this study, the bending, free vibration and buckling behaviours of FG microplates based on the MCST and four-variable refined plate and quasi-3D theories are investigated using IGA. While the MCST is employed to capture the small-scale effects, the displacement fields of those microplates are expressed based on a novel seventh-order refined plate theory and quasi-3D theory. The mechanical behaviour of FG microplates is then analysed by this IGA in which NURBS functions are simultaneously used to exactly describe the geometry and construct the basis functions of the approximations. It is worth mentioning that even though NURBS may not fully perform their ability to describe geometry exactly since the plate's domains investigated in this study are not highly complex, NURBS far outweigh traditional FEA in the higher-order derivative of approximations which are essentially required

in the proposed RPT and MCST.

The outline of this study is as follows. The next section presents theories which are applicable for analysis of FG microplates including MCST, RPT and quasi-3D theory. In addition, a brief note on FGMs is also introduced in this section. Section 3 focuses on the IGA and NURBS-based formulation of the quasi-3D theory. The numerical examples which cover static bending, free vibration and buckling analysis of rectangular and circular FG microplates with various boundary conditions are provided in Section 4. Finally, conclusions are given in Section 5.

2. A novel theory for FG microplates

In this section, a brief review on the formulation of the MCST with only one material length scale that accounts for size-dependent effects is presented. It is followed by the definitions required to describe FGMs of which the studied microplates are made. The displacement field of these plates is then derived based on the four-variable refined plate theory and quasi-3D plate theory where a novel seventh-order shear deformation theory is proposed.

2.1. Modified couple stress theory

According to the MCST which is proposed by Yang et al. [24], the strain energy density w for linear isotropic material is a quadratic function of generalised strains

$$w = \frac{1}{2}\lambda \left(\mathrm{tr}\boldsymbol{\varepsilon}\right)^2 + \mu \left(\boldsymbol{\varepsilon} : \boldsymbol{\varepsilon} + \ell^2 \boldsymbol{\chi} : \boldsymbol{\chi}\right), \tag{1}$$

where λ and μ are Lamé's constants, μ is also known as shear modulus which is often denoted as G, ℓ represents material length scale parameter and the strain tensor $\boldsymbol{\varepsilon}$ and symmetric curvature tensor $\boldsymbol{\chi}$ are defined by

$$\boldsymbol{\varepsilon} = \frac{1}{2}\left[\nabla \mathbf{u} + (\nabla \mathbf{u})^T\right], \tag{2a}$$

$$\boldsymbol{\chi} = \frac{1}{2}\left[\nabla \boldsymbol{\theta} + (\nabla \boldsymbol{\theta})^T\right], \tag{2b}$$

where $\mathbf{u}$ is the displacement vector and the rotation vector $\boldsymbol{\theta}$ is given by

$$\boldsymbol{\theta} = \frac{1}{2}\mathrm{curl}\left(\mathbf{u}\right). \tag{3}$$

The strain energy U stored in a deformed elastic body is then defined as

$$U = \int_V w dV = \int_V \left(\boldsymbol{\sigma} : \boldsymbol{\varepsilon} + \mathbf{m} : \boldsymbol{\chi}\right) dV, \tag{4}$$

where $\boldsymbol{\sigma}$ and $\mathbf{m}$ are the symmetric stress tensor and the deviatoric part of the symmetric couple stress tensor, respectively. These components, $\boldsymbol{\sigma}$ and $\mathbf{m}$, which are conjugated to the deformation measures $\boldsymbol{\varepsilon}$ and $\boldsymbol{\chi}$, respectively, are given as

$$\boldsymbol{\sigma}(\boldsymbol{\varepsilon}) = \lambda(\mathrm{tr}\boldsymbol{\varepsilon})\mathbf{I} + 2\mu\boldsymbol{\varepsilon}, \tag{5a}$$

$$\mathbf{m}(\boldsymbol{\chi}) = 2\mu\ell^2\boldsymbol{\chi}, \tag{5b}$$

where $\mathbf{I}$ is the identity tensor. Apparently, only one material length scale needed and the deviatoric couple stress tensor $\mathbf{m}$ is also symmetric, from which the MCST is formed.

2.2. Functionally graded material

The model configuration of a FGM which is made of metal and ceramic is illustrated in Fig. 1. There are several homogeneous models that are employed to estimate the effective properties of the FGMs. According to the rule of mixtures, the corresponding effective properties of these FGMs can be expressed as follows

$$P_e = P_m V_m + P_c V_c, \tag{6}$$

where P_m and P_c are the material properties of the metalic and ceramic phases, respectively, including the Young's modulus E, the density ρ and the Poisson's ratio ν. Meanwhile, V_m and V_c represent the volume fraction of metal and ceramic phases, respectively, which are defined as follows [8]

$$V_c(z) = \left(\frac{1}{2} + \frac{z}{h}\right)^n, \quad V_m = 1 - V_c, \quad -\frac{h}{2} \le z \le \frac{h}{2}, \tag{7}$$

where n is the material index. This equation implies a smooth variation in material properties governed by the material index n. As can be inferred from Eq. (7), $n = 0$ leads to a homogeneous ceramic material while a fully metalic material is obtained as n approaches $+\infty$.

Nevertheless, the rule of mixtures fails to describe the interaction between the material phases [77, 78]. Therefore, the Mori-Tanaka scheme [79, 80] was developed which integrates the effective bulk modulus K_e and shear modulus G_e are given by

$$\frac{K_e - K_m}{K_c - K_m} = \frac{V_c}{1 + V_m \frac{K_c - K_m}{K_m + \frac{4}{3}G_m}}, \quad \frac{G_e - G_m}{G_c - G_m} = \frac{V_c}{1 + V_m \frac{G_c - G_m}{G_m + f_1}}, \tag{8}$$

where

$$f_1 = \frac{G_m(9K_m + 8G_m)}{6(K_m + 2G_m)}. \tag{9}$$

The effective Young's modulus E_e and Poisson's ratio ν_e are then defined as

$$E_e = \frac{9K_eG_e}{3K_e + G_e}, \quad \nu_e = \frac{3K_e - 2G_e}{2(3K_e + G_e)}. \tag{10}$$

The variation in effective Young's modulus of Al/Al_2O_3 estimated by the rule of mixtures and Mori-Tanaka scheme is depicted in Fig. 2. As can be seen, the effective material property of the FGM varies continuously from the metal-rich surface at the bottom to the ceramic-rich surface at the top of the plate.

2.3. A novel seventh-order shear deformation plate theory

With regard to the plate theories, the third-order shear deformation model initially proposed by Reddy [53] is widely considered as a reliable theory in which no shear correction factor is required. In Reddy's theory, the displacement field, for $z \in [-h/2; h/2]$, is defined as

$$u(x,y,z) = u_0(x,y) + z\beta_x(x,y) + g(z)\Big(\beta_x(x,y) + w_{,x}(x,y)\Big), \tag{11a}$$

$$v(x,y,z) = v_0(x,y) + z\beta_y(x,y) + g(z)\Big(\beta_y(x,y) + w_{,y}(x,y)\Big), \tag{11b}$$

$$w(x,y,z) = w_0(x,y), \tag{11c}$$

where the comma notation $(_{,x},_{,y})$ indicates a derivative with respect to the spatial variable, $g(z) = -4z^3/(3h^2)$ [53] and the variables $\mathbf{u}_0 = [u_0 \quad v_0]^T$, w_0, and $\boldsymbol{\beta} = [\beta_x \quad \beta_y]^T$ are the membrane displacements, the transverse deflection of the mid-plane surface, and the rotations, respectively. By making further assumptions, $w_0 = w_b + w_s, \beta_x = -w_{b,x}, \beta_y = -w_{b,y}$, to Reddy's theory which contains five unknowns, Senthilnathan [56] proposed the four-variable refined plate theory which can be expressed in the generalised form as

$$u(x,y,z) = u_0(x,y) - zw_{b,x}(x,y) + g(z)\,w_{s,x}(x,y), \tag{12a}$$

$$v(x,y,z) = v_0(x,y) - zw_{b,y}(x,y) + g(z)\,w_{s,y}(x,y), \tag{12b}$$

$$w(x,y,z) = w_b(x,y) + w_s(x,y), \tag{12c}$$

where w_b and w_s represent bending and shear components of transverse displacement, respectively. The function $g : z \longmapsto g(z) = f(z) - z$ is employed to describe the distribution of transverse shear strains and stresses through the plate's thickness. It is necessary to have the first derivative of f satisfies the tangential zero value at $z = \pm h/2$ such that the traction-free condition at top and bottom surfaces is met. Consequently, the shear correction factor is no longer required for higher-order shear deformation theory and refined plate theory.

It should be noted that both the higher-order shear deformation theory and refined plate theory fail to capture the thickness stretching effect of normal deformation ($\varepsilon_z \neq 0$) due to the constant deflection through the plate thickness which can be inferred from Eq. (12c). In order to bypass this shortcoming, a number of theories which consider the thickness stretching effect have been developed [81–83]. Zenkour [84, 85] proposed the four-variable quasi-3D plate theory accounting for both transverse shear and normal deformations which can be alternatively expressed as follows

$$u(x,y,z) = u_0(x,y) - zw_{b,x}(x,y) + f(z)\,w_{s,x}(x,y), \tag{13a}$$

$$v(x,y,z) = v_0(x,y) - zw_{b,y}(x,y) + f(z)\,w_{s,y}(x,y), \tag{13b}$$

$$w(x,y,z) = w_b(x,y) + \phi(z)\,w_s(x,y). \tag{13c}$$

As can be observed, this quasi-3D model has a similar form to that of the four-variable refined plate theory shown in Eq. (12). Indeed, the displacement field based on the refined

plate theory can be readily obtained by simplifying those of quasi-3D theory in which f and ϕ are replaced by g and 1, respectively. In addition, this formulation of quasi-3D displacement field requires less number of unknowns than that of existing theories [86–88]. It is worth noting that although, by the theoretical material models, the neutral plane of the functionally graded plate would not perfectly coincide with its mid-plane, the assumption of their coincidence which is widely used is applied in the above displacement fields.

A number of distribution functions, f and ϕ, are available for FGM plates based on higher-order shear deformation theory, refined plate theory, and quasi-3D plate theory. One may find the general framework to construct such polynomial functions in the recent work of Nguyen et al. [89]. In this study, a novel seventh-order function of f and its corresponding function ϕ are proposed for the four-variable refined plate theory and quasi-3D theory. The function f which represents the nonlinear distribution of the transverse shear strains and stresses is carefully chosen to satisfy the traction-free boundary conditions, therefore no shear correction factor is required for this refined plate theory. In addition, the function's coefficients are obtained by conducting optimisation procedure in which the minimisation of the differences between the outcome results and the existing analytical solutions is considered as objective functions and the coefficients play roles of design variables. The proposed functions of f and ϕ are presented in Table 1 and Fig. 3 along with others existing in the literature.

According to the displacement field and the strain-displacement relation, which are presented in Eqs. (13) and (2a), respectively, the following strain expressions can be obtained as

$$\boldsymbol{\varepsilon}\left(x,y,z\right)=\boldsymbol{\varepsilon}_0+z\boldsymbol{\kappa}_b+f\left(z\right)\boldsymbol{\kappa}_s, \tag{14a}$$

$$\boldsymbol{\gamma}\left(x,y,z\right)=\left[f'\left(z\right)+\phi\left(z\right)\right]\boldsymbol{\varepsilon}_s, \tag{14b}$$

where

$$\begin{aligned}
&\boldsymbol{\varepsilon}=\begin{bmatrix}\varepsilon_x\\ \varepsilon_y\\ \gamma_{xy}\end{bmatrix},\quad \boldsymbol{\varepsilon}_0=\begin{bmatrix}u_{0,x}\\ v_{0,y}\\ u_{0,y}+v_{0,x}\end{bmatrix},\quad \boldsymbol{\kappa}_b=-\begin{bmatrix}w_{b,xx}\\ w_{b,yy}\\ 2w_{b,xy}\end{bmatrix},\quad \boldsymbol{\kappa}_s=\begin{bmatrix}w_{s,xx}\\ w_{s,yy}\\ 2w_{s,xy}\end{bmatrix},\\
&\boldsymbol{\gamma}=\begin{bmatrix}\gamma_{xz}\\ \gamma_{yz}\end{bmatrix},\quad \boldsymbol{\varepsilon}_s=\begin{bmatrix}w_{s,x}\\ w_{s,y}\end{bmatrix},\quad \varepsilon_z=\phi'\left(z\right)w_s.
\end{aligned} \tag{15}$$

Using Eqs. (13), (3), and (2b), the rotation vector and the curvature vector are expressed as

$$\boldsymbol{\theta}=\begin{bmatrix}\theta_x\\ \theta_y\\ \theta_z\end{bmatrix}=\frac{1}{2}\begin{bmatrix}2w_{b,y}-\left(f'-\phi\right)w_{s,y}\\ -2w_{b,x}+\left(f'-\phi\right)w_{s,x}\\ v_{0,x}-u_{0,y}\end{bmatrix}, \tag{16a}$$

$$\boldsymbol{\chi}=\begin{bmatrix}\boldsymbol{\chi}_b\\ \boldsymbol{\chi}_s\\ \chi_{zz}\end{bmatrix}=\begin{bmatrix}\boldsymbol{\chi}_{b0}\\ \boldsymbol{\chi}_{s0}\\ 0\end{bmatrix}+\begin{bmatrix}f'\boldsymbol{\chi}_{b1}\\ f''\boldsymbol{\chi}_{s2}\\ 0\end{bmatrix}+\begin{bmatrix}\phi\boldsymbol{\chi}_{b3}\\ \phi'\boldsymbol{\chi}_{s4}\\ 0\end{bmatrix}, \tag{16b}$$

where

$$\boldsymbol{\chi}_b = \begin{bmatrix} \chi_{xx} \\ \chi_{yy} \\ \chi_{xy} \end{bmatrix}, \boldsymbol{\chi}_{b0} = \frac{1}{2}\begin{bmatrix} w_{b,xy} \\ -w_{b,xy} \\ w_{b,yy} - w_{b,xx} \end{bmatrix}, \boldsymbol{\chi}_{b1} = \frac{1}{4}\begin{bmatrix} -2w_{s,xy} \\ 2w_{s,xy} \\ -w_{s,yy} + w_{s,xx} \end{bmatrix}, \boldsymbol{\chi}_{b3} = \frac{1}{4}\begin{bmatrix} 2w_{s,xy} \\ -2w_{s,xy} \\ w_{s,yy} - w_{s,xx} \end{bmatrix},$$
$$\boldsymbol{\chi}_s = \begin{bmatrix} \chi_{xz} \\ \chi_{yz} \end{bmatrix}, \boldsymbol{\chi}_{s0} = \frac{1}{4}\begin{bmatrix} v_{0,xx} - u_{0,xy} \\ v_{0,xy} - u_{0,yy} \end{bmatrix}, \boldsymbol{\chi}_{s2} = \frac{1}{4}\begin{bmatrix} -w_{s,y} \\ w_{s,x} \end{bmatrix}, \boldsymbol{\chi}_{s4} = \frac{1}{4}\begin{bmatrix} w_{s,y} \\ -w_{s,x} \end{bmatrix}. \tag{17}$$

According to Eq. (5), the constitutive relations for classical and modified couple stress theories can be presented in an explicit form as

$$\begin{Bmatrix} \sigma_x \\ \sigma_y \\ \sigma_z \\ \sigma_{xy} \\ \tau_{xz} \\ \tau_{yz} \end{Bmatrix} = \begin{bmatrix} Q_{11} & Q_{12} & Q_{13} & 0 & 0 & 0 \\ & Q_{22} & Q_{23} & 0 & 0 & 0 \\ & & Q_{33} & 0 & 0 & 0 \\ & & & Q_{66} & 0 & 0 \\ & & & & Q_{55} & 0 \\ \text{sym.} & & & & & Q_{44} \end{bmatrix} \begin{Bmatrix} \varepsilon_x \\ \varepsilon_y \\ \varepsilon_z \\ \varepsilon_{xy} \\ \gamma_{xz} \\ \gamma_{yz} \end{Bmatrix}, \tag{18a}$$

$$m_{ij} = 2G_e\ell^2\chi_{ij}, \tag{18b}$$

where, for the proposed quasi-3D theory ($\varepsilon_z \neq 0$), Q_{ij} are the three-dimensional elastic constants which write

$$\begin{aligned} Q_{11} = Q_{22} = Q_{33} &= \frac{(1-\nu_e)\,E_e}{(1-2\nu_e)\,(1+\nu_e)}, \\ Q_{12} = Q_{13} = Q_{23} &= \frac{\nu_e E_e}{(1-2\nu_e)\,(1+\nu_e)}, \\ Q_{44} = Q_{55} = Q_{66} &= \frac{E_e}{2\,(1+\nu_e)}, \end{aligned} \tag{19}$$

meanwhile, for the proposed refined plate theory ($\varepsilon_z = 0$), Q_{ij} are reduced plane-stress elastic constants and are expressed as

$$\begin{aligned} Q_{11} = Q_{22} &= \frac{E_e}{1-\nu_e^2}, \\ Q_{12} = Q_{21} &= \frac{E_e\nu_e}{1-\nu_e^2}, \\ Q_{44} = Q_{55} = Q_{66} &= \frac{E_e}{2\,(1+\nu_e)}, \end{aligned} \tag{20}$$

and the shear modulus $G_e = \dfrac{E_e}{2(1+\nu_e)}$.

In this study, the weak form of the static bending, vibration, and buckling problems are derived using the Hamilton's principle and weak formulation. One can find details on those

well-known procedures in the literature [63, 90, 91]. Firstly, the weak form of the static bending of the couple-stress-based microplates subjected to transverse load loading q_0 can be expressed in the following compact form

$$\begin{aligned}\int_{\Omega}\delta\boldsymbol{\varepsilon}_b^T\mathbf{D}^b\boldsymbol{\varepsilon}_b d\Omega+\int_{\Omega}\delta\boldsymbol{\varepsilon}_s^T\mathbf{D}^s\boldsymbol{\varepsilon}_s d\Omega+\int_{\Omega}\delta\left(\boldsymbol{\chi}_b^c\right)^T\boldsymbol{D}_c^b\boldsymbol{\chi}_b^c d\Omega+\int_{\Omega}\delta\left(\boldsymbol{\chi}_s^c\right)^T\mathbf{D}_c^s\boldsymbol{\chi}_s^c d\Omega \\ =\int_{\Omega}\left[\delta w_b+\phi\left(\frac{h}{2}\right)\delta w_s\right]q_0 d\Omega\end{aligned}, \tag{21}$$

where the strain tensors and material matrices in the first two terms in Eq. (21) related to classical elastic theory are

$$\boldsymbol{\varepsilon}_b=\begin{bmatrix}\boldsymbol{\varepsilon}_0\\ \boldsymbol{\kappa}_b\\ \boldsymbol{\kappa}_s\\ w_s\end{bmatrix},\quad \boldsymbol{\varepsilon}_s=\begin{bmatrix}w_{s,x}\\ w_{s,y}\end{bmatrix},\quad \mathbf{D}^b=\begin{bmatrix}\mathbf{A}&\mathbf{B}&\mathbf{E}&\mathbf{X}\\ \mathbf{B}&\mathbf{D}&\mathbf{F}&\mathbf{Y}^b\\ \mathbf{E}&\mathbf{F}&\mathbf{H}&\mathbf{Y}^s\\ \mathbf{X}&\mathbf{Y}^b&\mathbf{Y}^s&Z_{33}\end{bmatrix}, \tag{22}$$

in which the material matrices are calculated by

$$(\mathbf{A},\mathbf{B},\mathbf{D},\mathbf{E},\mathbf{F},\mathbf{H})=\int_{-h/2}^{h/2}\left[1,z,z^2,f(z),zf(z),f^2(z)\right]\bar{\mathbf{Q}}dz, \tag{23a}$$

$$\left(\mathbf{X},\mathbf{Y}^b,\mathbf{Y}^s\right)=\int_{-h/2}^{h/2}\left[\phi'(z),z\phi'(z),f(z)\phi'(z)\right]\tilde{\mathbf{Q}}dz, \tag{23b}$$

$$Z_{33}=\int_{-h/2}^{h/2}\left[\phi'(z)\right]^2 Q_{33}dz, \tag{23c}$$

$$\mathbf{D}^s=\int_{-h/2}^{h/2}\left[f'(z)+\phi(z)\right]^2\hat{\mathbf{Q}}dz, \tag{23d}$$

$$\bar{\mathbf{Q}}=\begin{bmatrix}Q_{11}&Q_{12}&0\\ Q_{21}&Q_{22}&0\\ 0&0&Q_{66}\end{bmatrix},\quad \tilde{\mathbf{Q}}=\begin{bmatrix}Q_{13}\\ Q_{23}\\ 0\end{bmatrix},\quad \hat{\mathbf{Q}}=\begin{bmatrix}Q_{44}&0\\ 0&Q_{55}\end{bmatrix}, \tag{23e}$$

and where the curvature tensors and material matrices in the third and fourth terms in Eq. (21) representing the couple stress theory are

$$\boldsymbol{\chi}_b^c=\begin{bmatrix}\boldsymbol{\chi}_{b0}\\ \boldsymbol{\chi}_{b1}\\ \boldsymbol{\chi}_{b3}\end{bmatrix},\quad \boldsymbol{\chi}_s^c=\begin{bmatrix}\boldsymbol{\chi}_{s0}\\ \boldsymbol{\chi}_{s2}\\ \boldsymbol{\chi}_{s4}\end{bmatrix},\quad \mathbf{D}_c^b=\begin{bmatrix}\mathbf{A}^c&\mathbf{B}^c&\mathbf{E}^c\\ \mathbf{B}^c&\mathbf{D}^c&\mathbf{F}^c\\ \mathbf{E}^c&\mathbf{F}^c&\mathbf{H}^c\end{bmatrix},\quad \mathbf{D}_c^s=\begin{bmatrix}\mathbf{X}^c&\mathbf{Y}^c&\mathbf{T}^c\\ \mathbf{Y}^c&\mathbf{Z}^c&\mathbf{V}^c\\ \mathbf{T}^c&\mathbf{V}^c&\mathbf{W}^c\end{bmatrix}, \tag{24}$$

in which the material matrices are be defined as

$$(\mathbf{A}^c, \mathbf{B}^c, \mathbf{D}^c, \mathbf{E}^c, \mathbf{F}^c, \mathbf{H}^c) = \int_{-h/2}^{h/2} \left(1, f'(z), [f'(z)]^2, \phi(z), f'(z)\phi(z), [\phi(z)]^2\right) \bar{\mathbf{G}} dz, \quad (25a)$$

$$(\mathbf{X}^c, \mathbf{Y}^c, \mathbf{Z}^c, \mathbf{T}^c, \mathbf{V}^c, \mathbf{W}^c) = \int_{-h/2}^{h/2} \left(1, f''(z), [f''(z)]^2, \phi'(z), f''(z)\phi'(z), [\phi'(z)]^2\right) \hat{\mathbf{G}} dz, \quad (25b)$$

where

$$\bar{\mathbf{G}} = 2G_e\ell^2 \begin{bmatrix} 1 & 0 & 0 \\ 0 & 1 & 0 \\ 0 & 0 & 1 \end{bmatrix}, \quad \hat{\mathbf{G}} = 2G_e\ell^2 \begin{bmatrix} 1 & 0 \\ 0 & 1 \end{bmatrix}. \quad (26)$$

The weak form of the free vibration of the couple-stress-based microplates is briefly expressed as

$$\int_\Omega \delta\boldsymbol{\varepsilon}_b^T \mathbf{D}^b \boldsymbol{\varepsilon}_b d\Omega + \int_\Omega \delta\boldsymbol{\varepsilon}_s^T \mathbf{D}^s \boldsymbol{\varepsilon}_s d\Omega + \int_\Omega \delta(\boldsymbol{\chi}_b^c)^T \mathbf{D}_c^b \boldsymbol{\chi}_b^c d\Omega + \int_\Omega \delta(\boldsymbol{\chi}_s^c)^T \mathbf{D}_c^s \boldsymbol{\chi}_s^c d\Omega = \int_\Omega \delta\tilde{\mathbf{u}}^T \tilde{\mathbf{m}} \ddot{\tilde{\mathbf{u}}} d\Omega, \quad (27)$$

where $\tilde{\mathbf{u}} = [u_0 \quad -w_{b,x} \quad w_{s,x} \quad v_0 \quad -w_{b,y} \quad w_{s,y} \quad w_b \quad w_s \quad 0]^T$, and the mass matrix $\tilde{\mathbf{m}}$ is defined by

$$\tilde{\mathbf{m}} = \begin{bmatrix} \mathbf{I}_0 & 0 & 0 \\ 0 & \mathbf{I}_0 & 0 \\ 0 & 0 & \mathbf{I}_1 \end{bmatrix} \quad \text{in which} \quad \mathbf{I}_0 = \begin{bmatrix} I_1 & I_2 & I_4 \\ I_2 & I_3 & I_5 \\ I_4 & I_5 & I_6 \end{bmatrix}, \quad \mathbf{I}_1 = \begin{bmatrix} I_1 & I_7 & 0 \\ I_7 & I_8 & 0 \\ 0 & 0 & 0 \end{bmatrix}, \quad (28a)$$

$$(I_1, I_2, I_3, I_4, I_5, I_6, I_7, I_8) = \int_{-h/2}^{h/2} \rho\left[1, z, z^2, f(z), zf(z), f^2(z), \phi(z), \phi^2(z)\right] dz. \quad (28b)$$

For buckling analysis, the weak form of the couple-stress-based microplates subjected to in-plane loading is of the form

$$\begin{aligned} \int_\Omega \delta\boldsymbol{\varepsilon}_b^T \mathbf{D}^b \boldsymbol{\varepsilon}_b d\Omega + \int_\Omega \delta\boldsymbol{\varepsilon}_s^T \mathbf{D}^s \boldsymbol{\varepsilon}_s d\Omega + \int_\Omega \delta(\boldsymbol{\chi}_b^c)^T \mathbf{D}_c^b \boldsymbol{\chi}_b^c d\Omega + \int_\Omega \delta(\boldsymbol{\chi}_s^c)^T \mathbf{D}_c^s \boldsymbol{\chi}_s^c d\Omega \\ + \int_\Omega \nabla^T \delta[w_b + \phi(0) w_s] \mathbf{N}_0 \nabla[w_b + \phi(0) w_s] d\Omega = 0 \end{aligned}, \quad (29)$$

where $\nabla^T = [\partial/\partial x \quad \partial/\partial y]^T$ and $\mathbf{N}_0 = \begin{bmatrix} N_x^0 & N_{xy}^0 \\ N_{xy}^0 & N_y^0 \end{bmatrix}$ are the transpose of gradient operator and matrix of pre-buckling loads, respectively.

3. FG microplate formulation based on NURBS basis functions

In this section, a brief review on NURBS which serves as the basis functions of IGA will be presented. It is followed by a novel NURBS-based formulation for couple-stress microplate bending, free vibration and buckling that rely upon the refined plate theory and the quasi-3D theory.

3.1. B-splines and NURBS basis functions

The starting point to express NURBS basis functions is a non-decreasing knot vector $\boldsymbol{\Xi} = \{\xi_1, \xi_2, ..., \xi_{n+p+1}\}$ where the i^{th} knot $\xi_i \in \mathbb{R}$, n represents the number of basis functions, and p denotes the polynomial order. The knot vectors can be either uniform if the knots are equally spaced in the parameter space or open if its first and last knot values are repeated $p+1$ times. The knot spans which are bounded by knots define element domains.

The B-spline basis functions that are constructed by the Cox-de Boor recursion formula, starting with the zeroth order ($p = 0$) are defined by [61, 62]

$$N_{i,0}(\xi) = \begin{cases} 1 & \text{if} \quad \xi_i \leq \xi < \xi_{i+1}, \\ 0 & \text{otherwise}, \end{cases} \tag{30a}$$

$$N_{i,p}(\xi) = \frac{\xi - \xi_i}{\xi_{i+p} - \xi_i} N_{i,p-1}(\xi) + \frac{\xi_{i+p+1} - \xi}{\xi_{i+p+1} - \xi_{i+1}} N_{i+1,p-1}(\xi), \text{for } p \geq 1, \tag{30b}$$

in which the fraction 0/0 is defined as zero. While the basis functions are smooth, e.g. C^∞ continuity, within this domain, they are C^{p-k} continuous across the knots, where k is the multiplicity of the knot. Therefore, for $p \geq 2$, the basis functions are of C^1 continuous at each knot with single multiplicity (single knot) and at the boundary of the know span. Two-dimensional B-splines are obtained by introducing a second knot vector $\mathbf{H} = \{\eta_1, \eta_2, ..., \eta_{m+q+1}\}$, where m and q are the number of basis functions and the polynomial in η direction, respectively, and using the tensor product of $\boldsymbol{\Xi}$ and $\mathbf{H}$ in the parametric dimensions yielding

$$N_A(\xi, \eta) = N_{i,p}(\xi) M_{j,q}(\eta). \tag{31}$$

For illustration purposes, Fig. 4 depicts the one- and two-dimensional B-spline basis functions which are generated from the knot vector $\boldsymbol{\Xi} = \{0, 0, 0, 0, 1/5, 2/5, 3/5, 3/5, 3/5, 4/5, 1, 1, 1, 1\}$ and its combination with the knot vector $\mathbf{H} = \{0, 0, 0, 1/4, 1/2, 3/4, 1, 1, 1\}$, respectively.

The non-uniform rational B-splines (NURBS) basis functions are then further defined by providing an additional weight ζ_A to each control point given by [62]

$$R_A(\xi, \eta) = \frac{N_A \zeta_A}{\sum_{\hat{A}}^{n \times m} N_{\hat{A}}(\xi, \eta) \zeta_{\hat{A}}}. \tag{32}$$

It is noted that B-splines basis function are special cases of NURBS function. Indeed, if all the individual weights corresponding the control points are assigned an equal constant, the NURBS function degenerates to a B-spline function.

3.2. A novel NURBS-based formulation of modified couple stress theory

By using NURBS basis functions, the displacement variables $\mathbf{u}$ of a microplate can be approximately calculated as follows

$$\mathbf{u}^h(\xi,\eta)=\sum_{A=1}^{n\times m}R_A(\xi,\eta)\mathbf{q}_A, \tag{33}$$

where $n\times m$ is the number of basis functions and $\mathbf{q}_A=[u_{0A}\quad v_{0A}\quad w_{bA}\quad w_{sA}]^T$ denotes the vector of degrees of freedom associated with the control point A. By substituting the approximations Eq. (33) into the strain-displacement relations Eq. (15), the in-plane and shear strains can be obtained

$$\begin{bmatrix}\boldsymbol{\varepsilon}_0^T & \boldsymbol{\kappa}_b^T & \boldsymbol{\kappa}_s^T & \boldsymbol{\varepsilon}_s^T\end{bmatrix}^T=\sum_{A=1}^{n\times m}\begin{bmatrix}(\mathbf{B}_A^m)^T & \left(\mathbf{B}_A^{b1}\right)^T & \left(\mathbf{B}_A^{b2}\right)^T & (\mathbf{B}_A^s)^T\end{bmatrix}^T\mathbf{q}_A, \tag{34}$$

where

$$\begin{aligned}\mathbf{B}_A^m&=\begin{bmatrix}R_{A,x}&0&0&0\\0&R_{A,y}&0&0\\R_{A,y}&R_{A,x}&0&0\end{bmatrix},\quad \mathbf{B}_A^{b1}=-\begin{bmatrix}0&0&R_{A,xx}&0\\0&0&R_{A,yy}&0\\0&0&2R_{A,xy}&0\end{bmatrix},\\ \mathbf{B}_A^{b2}&=\begin{bmatrix}0&0&0&R_{A,xx}\\0&0&0&R_{A,yy}\\0&0&0&2R_{A,xy}\end{bmatrix},\quad \mathbf{B}_A^{s}=\begin{bmatrix}0&0&0&R_{A,x}\\0&0&0&R_{A,y}\end{bmatrix},\end{aligned} \tag{35}$$

and the curvatures are obtained by substituting Eq. (33) into Eq. (17) :

$$\begin{aligned}&\begin{bmatrix}\boldsymbol{\chi}_{b0}^T & \boldsymbol{\chi}_{b1}^T & \boldsymbol{\chi}_{b3}^T & \boldsymbol{\chi}_{s0}^T & \boldsymbol{\chi}_{s2}^T & \boldsymbol{\chi}_{s4}^T\end{bmatrix}^T\\ &=\sum_{A=1}^{n\times m}\begin{bmatrix}\left(\tilde{\mathbf{B}}_A^{b0}\right)^T & \left(\tilde{\mathbf{B}}_A^{b1}\right)^T & \left(\tilde{\mathbf{B}}_A^{b3}\right)^T & \left(\tilde{\mathbf{B}}_A^{s0}\right)^T & \left(\tilde{\mathbf{B}}_A^{s2}\right)^T & \left(\tilde{\mathbf{B}}_A^{s4}\right)^T\end{bmatrix}^T\mathbf{q}_A,\end{aligned} \tag{36}$$

where

$$\begin{aligned}\tilde{\mathbf{B}}_A^{b0}&=\frac{1}{2}\begin{bmatrix}0&0&2R_{A,xy}&0\\0&0&-2R_{A,xy}&0\\0&0&(-R_{A,xx}+R_{A,yy})&0\end{bmatrix},\quad \tilde{\mathbf{B}}_A^{b1}=\frac{1}{4}\begin{bmatrix}0&0&0&-2R_{A,xy}\\0&0&0&2R_{A,xy}\\0&0&0&(R_{A,xx}-R_{A,yy})\end{bmatrix},\\ \tilde{\mathbf{B}}_A^{b3}&=\frac{1}{4}\begin{bmatrix}0&0&0&2R_{A,xy}\\0&0&0&-2R_{A,xy}\\0&0&0&(-R_{A,xx}+R_{A,yy})\end{bmatrix},\quad \tilde{\mathbf{B}}_A^{s0}=\frac{1}{4}\begin{bmatrix}-R_{A,xy}&R_{A,xx}&0&0\\-R_{A,yy}&R_{A,xy}&0&0\end{bmatrix},\\ \tilde{\mathbf{B}}_A^{s2}&=\frac{1}{4}\begin{bmatrix}0&0&0&-R_{A,y}\\0&0&0&R_{A,x}\end{bmatrix},\quad \tilde{\mathbf{B}}_A^{s4}=\frac{1}{4}\begin{bmatrix}0&0&0&R_{A,y}\\0&0&0&-R_{A,x}\end{bmatrix}.\end{aligned} \tag{37}$$

Substituting Eqs. (34) and (36) into Eqs. (21), (27), and (29), the matrix form of the global equilibrium equations for static bending, free vibration, and buckling can be

respectively written as follows

$$\mathbf{K}\mathbf{q} = \mathbf{F}, \tag{38a}$$

$$\left(\mathbf{K} - \omega^2\mathbf{M}\right)\mathbf{q} = \mathbf{0}, \tag{38b}$$

$$\left(\mathbf{K} - \lambda_{cr}\mathbf{K}_g\right)\mathbf{q} = \mathbf{0}, \tag{38c}$$

where the global stiffness matrix $\mathbf{K}$ is the summation of the stiffness matrices corresponding to the classical theory $\mathbf{K}_s$ and the couple stress theory $\mathbf{K}_c$, i.e. $\mathbf{K} = \mathbf{K}_s + \mathbf{K}_c$. These matrices are calculated as follows

$$\mathbf{K}_s = \int_\Omega \left(\begin{Bmatrix} \mathbf{B}^m \\ \mathbf{B}^{b1} \\ \mathbf{B}^{b2} \\ \mathbf{B}^z \end{Bmatrix}^T \begin{bmatrix} \mathbf{A} & \mathbf{B} & \mathbf{E} & \mathbf{X} \\ \mathbf{B} & \mathbf{D} & \mathbf{F} & \mathbf{Y}^b \\ \mathbf{E} & \mathbf{F} & \mathbf{H} & \mathbf{Y}^s \\ \mathbf{X} & \mathbf{Y}^b & \mathbf{Y}^s & Z_{33} \end{bmatrix} \begin{Bmatrix} \mathbf{B}^m \\ \mathbf{B}^{b1} \\ \mathbf{B}^{b2} \\ \mathbf{B}^z \end{Bmatrix} + \left(\mathbf{B}^s\right)^T \mathbf{D}^s \mathbf{B}^s \right) d\Omega, \tag{39a}$$

$$\mathbf{K}_c = \int_\Omega \left(\begin{Bmatrix} \tilde{\mathbf{B}}^{b0} \\ \tilde{\mathbf{B}}^{b1} \\ \tilde{\mathbf{B}}^{b3} \end{Bmatrix}^T \begin{bmatrix} \mathbf{A}^c & \mathbf{B}^c & \mathbf{E}^c \\ \mathbf{B}^c & \mathbf{D}^c & \mathbf{F}^c \\ \mathbf{E}^c & \mathbf{F}^c & \mathbf{H}^c \end{bmatrix} \begin{Bmatrix} \tilde{\mathbf{B}}^{b0} \\ \tilde{\mathbf{B}}^{b1} \\ \tilde{\mathbf{B}}^{b3} \end{Bmatrix} + \begin{Bmatrix} \tilde{\mathbf{B}}^{s0} \\ \tilde{\mathbf{B}}^{s2} \\ \tilde{\mathbf{B}}^{s4} \end{Bmatrix}^T \begin{bmatrix} \mathbf{X}^c & \mathbf{Y}^c & \mathbf{T}^c \\ \mathbf{Y}^c & \mathbf{Z}^c & \mathbf{V}^c \\ \mathbf{T}^c & \mathbf{V}^c & \mathbf{W}^c \end{bmatrix} \begin{Bmatrix} \tilde{\mathbf{B}}^{s0} \\ \tilde{\mathbf{B}}^{s2} \\ \tilde{\mathbf{B}}^{s4} \end{Bmatrix} \right) d\Omega, \tag{39b}$$

in which $\mathbf{B}_A^z = \begin{bmatrix} 0 & 0 & 0 & R_A \end{bmatrix}$. The load vector $\mathbf{F}$ is given by

$$\mathbf{F} = \int_\Omega q_0 \mathbf{R} d\Omega, \tag{40}$$

where $\mathbf{R} = \begin{bmatrix} 0 & 0 & R_A & \phi\left(\frac{h}{2}\right) R_A \end{bmatrix}^T$, the global mass matrix is computed by

$$\mathbf{M} = \int_\Omega \tilde{\mathbf{R}}^T \tilde{\mathbf{m}} \tilde{\mathbf{R}} d\Omega, \tag{41}$$

in which $\tilde{\mathbf{R}} = \begin{Bmatrix} \mathbf{R}_1 & \mathbf{R}_2 & \mathbf{R}_3 \end{Bmatrix}^T$, where

$$\mathbf{R}_1 = \begin{bmatrix} R_A & 0 & 0 & 0 \\ 0 & 0 & -R_{A,x} & 0 \\ 0 & 0 & 0 & R_{A,x} \end{bmatrix}, \quad \mathbf{R}_2 = \begin{bmatrix} 0 & R_A & 0 & 0 \\ 0 & 0 & -R_{A,y} & 0 \\ 0 & 0 & 0 & R_{A,y} \end{bmatrix}, \quad \mathbf{R}_3 = \begin{bmatrix} 0 & 0 & R_A & 0 \\ 0 & 0 & 0 & R_A \\ 0 & 0 & 0 & 0 \end{bmatrix}, \tag{42}$$

the geometric stiffness matrix is given as

$$\mathbf{K}_g = \int_\Omega \left(\mathbf{B}^g\right)^T \mathbf{N}_0 \mathbf{B}^g d\Omega, \tag{43}$$

where

$$\mathbf{B}^g = \begin{bmatrix} 0 & 0 & R_{A,x} & \phi(0) R_{A,x} \\ 0 & 0 & R_{A,y} & \phi(0) R_{A,y} \end{bmatrix}, \tag{44}$$

and ω and λ_{cr} represent the natural frequency and the critical buckling value, respectively.

As can be observed from Eq. (39), by introducing the distribution function f, the four-variable refined plate theory and quasi-3D theory do not require any shear correction factor, which is usually needed if the first-order shear deformation theory is applied, to describe the transverse shear stresses satisfying traction-free conditions. In addition, the expressions of $\mathbf{B}$ and $\tilde{\mathbf{B}}$ matrices in Eqs. (35) and (37) show the employment of the second-order derivatives of the approximation functions R_A. Consequently, C^1 continuous approximations are required. This requirement may cause difficulties to finite element analysis which can be solved by using the mixed interpolation of tensorial components (MITC) or increasing the degrees of freedom to transform the C^1 problems to C^0 ones [46, 92, 93]. Apparently, these approaches results in higher number of variables and larger computational cost. However, within the platform of isogeometric analysis in which NURBS basis functions are employed, the C^1-continuity requirement is naturally satisfied for $p \geq 2$ since the basis functions are C^{p-1} continuous across knot spans, i.e. elements. Therefore, the NURBS-based IGA would be a prominent numerical approach to deal with the proposed four-unknown C^1 quasi-3D refined plate theory and modified couple stress theory.

4. Numerical examples and discussion

In this section, convergence and verification studies are conducted to demonstrate the accuracy of the novel approaches presented in Section 2 and 3. In order to illustrate the efficiency of IGA approach in dealing with the MCST, this section is then continued by the computational analysis of FG rectangular and circular microplates with various types of boundary conditions for static bending, free vibration and buckling problems. In these investigations, the FG microplates made of a mixture of metal and ceramic whose material properties are presented in Table 2 are used. Throughout the numerical examples, unless otherwise specified, the material length scale ℓ is chosen as 17.6×10^{-6}m which was suggested by Lam et al. [21]. There are two types of boundary conditions considered

Simply supported (S)

$v_0 = w_b = w_s = 0 \quad$ at $x = 0, a$

$u_0 = w_b = w_s = 0 \quad$ at $y = 0, b$

Clamped (C)

$u_0 = v_0 = w_b = w_s = 0$ and $w_{b,x} = w_{b,y} = w_{s,x} = w_{s,y} = 0$

It should be noted that, within a IGA approach, while the homogeneous boundary conditions corresponding to the displacement itself, e.g. u_0, v_0, w_b, w_s, are easily treated in a similar way to the traditional finite element method, those require the first derivative of the displacement components, e.g. $w_{b,x}, w_{b,y}, w_{s,x}, w_{s,y}$, can be enforced by assigning zero values to all displacements of control points which are directly related to clamped edges and their adjacent points [91, 94].

4.1. Convergence and verification studies

In order to evaluate the convergence and reliability of the approaches proposed in Sections 2 and 3, the MCST-based size-dependent analysis of homogeneous fully simply-supported

(SSSS) square microplate which is shown in Fig. 5 is conducted using RPT model. Moderately thick plates ($a/h = 20$) with four different values of material length scale ratio ($\ell/h = 0, 0.2, 0.6, 1$) are investigated. For each case, eight different finite element meshes are analysed to study the convergence rate of the proposed IGA approach. As can be seen from Table 3, while the fast convergence of the analysis for polynomial order $p = 3$ and $p = 4$ is obtained, solutions using quadratic polynomial $p = 2$ experience relatively slower convergence rate toward analytical solutions reported by Thai and Kim [40]. This agrees well with the expectation in which the higher polynomial functions give better solutions in terms of accuracy and convergence rate. Fig. 6 presents the convergence study with the relative error of non-dimensional central deflection of homogeneous square microplates with respect to the analytical solutions [40]. Based on the convergence study, the cubic ($p = 3$) NURBS element mesh of 11×11 is relatively sufficient for all analysis cases. Therefore, this mesh whose geometry is shown in Fig. 5 will be used throughout the next examples unless otherwise specified.

Further investigation on the accuracy of the proposed method is conducted using FG plates made of alumina and aluminum (Al/Al_2O_3). In this case, without considering couple stress effects, the proposed RPT ($\varepsilon_z = 0$) and quasi-3D ($\varepsilon_z \neq 0$) theories are applied to analyses of SSSS square plates using the rule of mixtures. The plates are subjected to uniformly and sinusoidally distributed loads which are defined as q_0 and $q_0 \sin\left(\frac{\pi x}{a}\right) \sin\left(\frac{\pi y}{a}\right)$, respectively. As can be observed in Table 4, the present results are in good agreement with those available in published works using various 2-D and quasi-3D theories. It should be noted that some numerical results generated from the proposed IGA approach using the distribution functions from other existing works [53, 84, 91] are also presented in the Table 4 . The above investigations confirm the validity and reliability of the proposed approaches.

4.2. Static bending analysis

In this section, the static bending analysis of FG microplates based on the MCST will be investigated. The SSSS square microplates are assumed to follow the rule of mixtures. The aspect ratio a/h, material length scale ratio ℓ/h, and material index n are taken into account. Table 5 presents the comparison of non-dimensional central deflection of an SSSS square plate with those of Thai and Kim [40]. While the results generated from the proposed RPT theory are in very good agreement, quasi-3D theory yields slightly different responses in terms of displacement. This is attributed to the consideration of the thickness stretching effect in the quasi-3D theory.

The bending responses of fully-clamped (CCCC) square Al/Al_2O_3 microplates under sinusoidally and uniformly distributed loads are further studied and presented in Table 6. It is noted that since no study on the static behaviours of CCCC microplates using MCST is reported in the literature, the results are compared with those generated from Reddy's HSDT model [53] using the proposed IGA approach. As can be seen, the results based on Reddy's model are in excellent agreement with the proposed RPT-based solutions. The effects of material index n and material length scale ℓ on the central displacement of a CCCC square Al/Al_2O_3 plate are depicted in Fig. 7 in which data are generated by the

proposed RPT and quasi-3D theories for three different ratios ℓ/h of 0, 0.4 and 1.0. As can be observed, an increase in the material index n leads to a rise of the plate's central deflection due to the decrease in the plate's stiffness. On the contrary, the growth of the material length scale ratio ℓ/h is followed by a decline in the displacement. In other words, for specific material length scale ℓ, the thinner the microplate, the higher plate's stiffness. It can be further observed that the discrepancy in terms of central deflection by the proposed RPT and quasi-3D is significantly decreased as ℓ/h increases and vanishes when $\ell/h = 1.0$. Fig. 8 depicts the deformed configurations of the Al/Al_2O_3 square microplates with various boundary conditions subjected to a sinusoidally distributed load in which $a/h, \ell/h$ and n are equal to $5, 0.4$ and 10, respectively. It should be noted that the deformed shapes of the microplates are scaled up for illustration purposes.

4.3. Free vibration analysis

In this part, the free vibration analysis of FG microplates based on a MCST is discussed. The proposed quasi-3D model is initially tested for linear elastic SSSS Al/ZrO_2-1 plates with various theories taking into account the normal shear deformation. It can be seen that the results given in Table 7 agree well with other published works. The proposed RPT and quasi-3D models using IGA are further tested for homogeneous square microplates. The results shown in Table 8 are compared with analytical solutions generated from CPT by Yin et al. [36] and TSDT by Thai and Kim [40] . As can be observed, while the proposed RPT model yields slight discrepancy with respect to Yin et al.'s [36] due to their CPT assumption neglecting shear deformations, it shows excellent agreement with Thai and Kim [40], especially as plates become thinner, i.e. a/h ratio is relatively large. Due to the consideration of the thickness stretching effects, the proposed quasi-3D model gives slightly different results in comparison with other theories which based on assumption of $\varepsilon_z = 0$.

Table 9 presents non-dimensional natural frequency of SSSS Al/Al_2O_3 square microplates. The results are compared with those of Thai and Kim [40] in which an analytical approach based on TSDT model is employed. Thick ($a/h = 5$), moderately thick ($a/h = 20$) and thin ($a/h = 100$) microplates are considered. The results reveal good agreement between the RPT and TSDT [40], especially when the material length scale ratio ℓ/h is small, e.g. 0 or 0.2. On the contrary, the discrepancy becomes larger as ℓ/h gets closer to 1. However, this phenomenon just happens for thick plates and tends to be less pronounced as the plates become thinner. Meanwhile, the quasi-3D gives slightly different results compared to that of RPT model. A general observation from Table 9 reveals that the higher material length scale ratio is chosen, the larger the natural frequencies of the plates the plate's stiffness increases. Fig. 9 presents the variation of the normalised natural frequency of CCCC Al/Al_2O_3 square microplate with respect to the material length scale parameter ratio ℓ/h, plate's aspect ratio a/h with different values of material index n. Fig. 10 provides a closer look at the effects of material index n and material length scale ratio ℓ/h on the plate's natural frequencies which are computed using the proposed RPT and quasi-3D models.

Similar to the previous case of bending analysis, the plate's stiffness decreases as a result of rising in material index n and decreasing material length scale ratio ℓ/h which leads to a decrease in natural frequency of the plate. In addition, the discrepancy in terms of frequency

results predicted by the proposed RPT and quasi-3D becomes less significant as ℓ/h gets bigger and almost vanish difference when $\ell/h = 1.0$. The first six natural frequencies of Al/Al_2O_3 square microplates with different types of boundary conditions are given in Table 10 in which the results are generated for $n = 1$ and $\ell/h = 0.2$. The present quasi-3D results show good agreement with those of Zenkour's quasi-3D model [84] using the proposed IGA approach. The first six mode shapes corresponding to the quasi-3D vibration analysis of CCCC microplates with $a/h = 10$ are presented in Fig. 11.

In the next step, free vibration of circular plates whose geometry configuration and mesh are shown in Fig. 12 will be investigated. Since there is no publication on the vibration behaviours of FG circular microplates based on the MCST, the investigation of circular plates in this study can serve as benchmark examples. Table 11 presents the fundamental natural frequencies which are firstly tested for homogeneous plates. Natural frequencies of plates without considering size-dependent effects ($l = 0$) are compared with results reported by Mohammadi et al. [95] and Nguyen et al. [91]. The results show very good agreement between the theories, especially proposed RPT and Nguyen et al.'s [91] which also uses another polynomial-based RPT model. Table 12 presents the first six natural frequencies of Al/Al_2O_3 circular plates with simple and clamped supports. The plate's thickness h and material index n are set as $0.2R$ and 1, respectively. As in the previous case of square microplates, Zenkour's quasi-3D model [84] using the proposed IGA approach is added for reference purpose since no study can be found for this problem in the literature. The first six vibration mode shapes of clamped plates with $\ell/h = 0.2$ using quasi-3D model are given in Fig. 13.

4.4. Buckling analysis

The buckling behaviour of square and circular FG microplates is discussed. In order to verify the proposed method and models in dealing with buckling analysis, the critical buckling load of SSSS FG microplates bearing biaxial loads is firstly calculated. The results are compared with analytical solutions based on the CPT and the FSDT by Thai and Choi [41] and refined plate theory by He et al. [45] for which material properties are $E_1 = 14.4$GPa, $\rho_1 = 12.2 \times 10^3$kg/m^3, $E_2 = 1.44$GPa, $\rho_2 = 1.22 \times 10^3$kg/m^3, $\nu_1 = \nu_2 = 0.38$. As can be seen in Table 13, although there is discrepancy for the case of thick microplates ($a/h = 5$), the results predicted by proposed RPT theory are in good agreement with those calculated by FSDT [41] and RPT [45] as plates become thinner. On the other hand, while CPT-based solutions are significantly different compared to that of FDST and RPTs due to the ignorance of shear deformations, especially for thick plates, the proposed quasi-3D theory which takes into account normal deformation yields similar results with respect to those of shear deformable theories of FSDT and RPTs.

Table 14 presents the biaxial buckling analysis results of Al/Al_2O_3 square microplates. The results are calculated based on the proposed RPT and quasi-3D theories which can serve as benchmark examples for future references since no result exists in the literature. The first six non-dimensional biaxial buckling loads of Al/Al_2O_3 square plates are reported in Table 15 for $n = 10$ and $\ell/h = 0.2$. While the results generated from the proposed quasi-3D and IGA-based Zenkour's quasi-3D theories [84] are relatively close to each other for both types

of boundary conditions, the RPT's show a clear discrepancy to the other theories, especially for the CCCC plates. This is due to the consideration of normal deformation of the quasi-3D theories. For $a/h = 5$, the first six buckling mode shapes of CCCC plates based on the proposed quasi-3D theory which are scaled up for illustration purposes are presented in Fig. 14.

Finally, this section ends with a number of investigations on buckling of circular FG microplates. Table 16 presents the results of the critical buckling loads of CCCC Al/ZrO_2-2 circular plates without considering couple stress effects. It should be noted that, for this particular attempt of comparison purpose, the material volume fractions are defined as $V_m = (0.5 - z/h)^n$ and $V_c = 1 - V_m$ [63, 96–98]. The comparison reveals that the results generated from proposed RPT are in good agreement with those of other shear deformation theories even with relatively thick and thick plates. The proposed quasi-3D approach yields slightly different results in all cases.

Table 17 presents the non-dimensional critical buckling loads of Al/Al_2O_3 circular microplates with various boundary conditions based on the proposed RPT and quasi-3D theories. The difference between the two theories is relatively small for both boundary conditions. The effects of the material index n and material length scale ratio ℓ/h on the critical buckling loads of simple and clamped supports of Al/Al_2O_3 circular microplates with $h/R = 0.2$ are illustrated in Fig. 15. Fig. 16 presents the variation of the normalised critical buckling loads of simply-supported Al/Al_2O_3 circular microplates with respect to the material length scale ratio ℓ/h and plate's aspect ratio a/h with different value of material index n.

The first six buckling loads of Al/Al_2O_3 circular microplates with various aspect ratios for $n = 1$ and $\ell/h = 0.6$ along with the results generated from Zenkour's quasi-3D theory [84] using proposed IGA approach are reported in Table 18. The first six buckling mode shapes corresponding to simply-supported circular microplates for $h/R = 0.2$ based on proposed quasi-3D theory are presented in Fig. 17.

5. Conclusions

In this study, a novel computational approach, based on the modified couple stress theory, the four-variable refined plate theory and the quasi-3D theory, and the NURBS-based isogeometric analysis, has been presented to investigate the static bending, free vibration, and buckling of functionally graded microplates with various geometries and boundary conditions. Within this proposed approach, the mathematical model governing the behaviour of the plates is constructed based on the modified couple stress theory with only one material length scale which efficiently accounts for the size dependency in small-scale structures. The novel seventh-order refined plate theory and quasi-3D theory with only four unknowns are also presented. This proposed quasi-3D approach not only considers shear deformations but also is able to accurately capture the thickness stretching effect which is neglected by other classical, higher-order shear deformation, and refined plate theories. The NURBS-based isogeometric analysis is used to exactly describe the geometry and approximately construct the unknown field in which the higher-order continuity requirement of the proposed kinematical and constitutive theories are readily satisfied. A number of investigations including novel

benchmark problems which have never been reported in the literature have confirmed the validity and efficiency of the proposed approach. The results also reveal that increase of the material length scale parameter ratio rises the microplate's stiffness which results in a decrease in the central displacement and an increase in the natural frequency and buckling load. On the contrary, an increase in the material index leads to the opposite effect in which the microplate's stiffness decreases. For all cases considered, the numerical results that are generated by the proposed refined plate theory and quasi-3D theory are slightly different due to the consideration of the thickness stretching effect. However, these discrepancies become less pronounced as the microplate becomes thinner.

Acknowledgement

The first and last authors gratefully acknowledge the financial support from the Northumbria University via the Researcher Development Framework.

References

[1] L. C. Trinh, T. P. Vo, A. I. Osofero, J. Lee, Fundamental frequency analysis of functionally graded sandwich beams based on the state space approach, Composite Structuresdoi:10.1016/j.compstruct.2015.11.010.

[2] T. P. Vo, H.-T. Thai, T.-K. Nguyen, A. Maheri, J. Lee, Finite element model for vibration and buckling of functionally graded sandwich beams based on a refined shear deformation theory, Engineering Structures 64 (2014) 12–22. doi:10.1016/j.engstruct.2014.01.029.

[3] T. P. Vo, H.-T. Thai, T.-K. Nguyen, F. Inam, Static and vibration analysis of functionally graded beams using refined shear deformation theory, Meccanica 49 (1) (2013) 155–168. doi:10.1007/s11012-013-9780-1.

[4] M. Asghari, M. T. Ahmadian, M. H. Kahrobaiyan, M. Rahaeifard, On the size-dependent behavior of functionally graded micro-beams, Materials & Design 31 (5) (2010) 2324–2329. doi:10.1016/j.matdes.2009.12.006.

[5] V.-H. Nguyen, T.-K. Nguyen, H.-T. Thai, T. P. Vo, A new inverse trigonometric shear deformation theory for isotropic and functionally graded sandwich plates, Composites Part B: Engineering 66 (2014) 233–246. doi:10.1016/j.compositesb.2014.05.012.

[6] H.-T. Thai, T. P. Vo, A new sinusoidal shear deformation theory for bending, buckling, and vibration of functionally graded plates, Applied Mathematical Modelling 37 (5) (2013) 3269–3281. doi:10.1016/j.apm.2012.08.008.

[7] S. Natarajan, S. Chakraborty, M. Thangavel, S. Bordas, T. Rabczuk, Size-dependent free flexural vibration behavior of functionally graded nanoplates, Computational Materials Science 65 (2012) 74–80. doi:10.1016/j.commatsci.2012.06.031.

[8] J. N. Reddy, Analysis of functionally graded plates, International Journal for Numerical Methods in Engineering 47 (1-3) (2000) 663–684. doi:10.1002/(SICI)1097-0207(20000110/30)47:1/3<663::AID-NME787>3.0.CO;2-8.

[9] J. L. Mantari, Refined and generalized hybrid type quasi-3d shear deformation theory for the bending analysis of functionally graded shells, Composites Part B: Engineering 83 (2015) 142–152. doi:10.1016/j.compositesb.2015.08.048.

[10] J. Torabi, Y. Kiani, M. R. Eslami, Linear thermal buckling analysis of truncated hybrid FGM conical shells, Composites Part B: Engineering 50 (2013) 265–272. doi:10.1016/j.compositesb.2013.02.025.

[11] F. Tornabene, Free vibration analysis of functionally graded conical, cylindrical shell and annular plate structures with a four-parameter power-law distribution, Computer Methods in Applied Mechanics and Engineering 198 (3740) (2009) 2911–2935. doi:10.1016/j.cma.2009.04.011.

[12] Y. Fu, H. Du, W. Huang, S. Zhang, M. Hu, TiNi-based thin films in MEMS applications: a review, Sensors and Actuators A: Physical 112 (23) (2004) 395–408. doi:10.1016/j.sna.2004.02.019.

[13] Z. Lee, C. Ophus, L. M. Fischer, N. Nelson-Fitzpatrick, K. L. Westra, S. Evoy, V. Radmilovic, U. Dahmen, D. Mitlin, Metallic NEMS components fabricated from nanocomposite AlMo films, Nanotechnology 17 (12) (2006) 3063. doi:10.1088/0957-4484/17/12/042.

[14] R. H. Baughman, C. Cui, A. A. Zakhidov, Z. Iqbal, J. N. Barisci, G. M. Spinks, G. G. Wallace, A. Mazzoldi, D. D. Rossi, A. G. Rinzler, O. Jaschinski, S. Roth, M. Kertesz, Carbon Nanotube Actuators, Science 284 (5418) (1999) 1340–1344. doi:10.1126/science.284.5418.1340.

[15] K.-T. Lau, H.-Y. Cheung, J. Lu, Y.-S. Yin, D. Hui, H.-L. Li, Carbon Nanotubes for Space and Bio-Engineering Applications, Journal of Computational and Theoretical Nanoscience 5 (1) (2008) 23–35. doi:10.1166/jctn.2008.003.

[16] S. J. V. Frankland, A. Caglar, D. W. Brenner, M. Griebel, Molecular Simulation of the Influence of Chemical Cross-Links on the Shear Strength of Carbon NanotubePolymer Interfaces, The Journal of Physical Chemistry B 106 (12) (2002) 3046–3048. doi:10.1021/jp015591+.

[17] K. M. Liew, X. Q. He, C. H. Wong, On the study of elastic and plastic properties of multi-walled carbon nanotubes under axial tension using molecular dynamics simulation, Acta Materialia 52 (9) (2004) 2521–2527. doi:10.1016/j.actamat.2004.01.043.

[18] A. Menk, S. Bordas, Influence of the microstructure on the stress state of solder joints during thermal cycling, in: 10th International Conference on Thermal, Mechanical and Multi-Physics simulation and Experiments in Microelectronics and Microsystems, 2009. EuroSimE 2009, 2009, pp. 1–5. doi:10.1109/ESIME.2009.4938405.

[19] N. A. Fleck, G. M. Muller, M. F. Ashby, J. W. Hutchinson, Strain gradient plasticity: Theory and experiment, Acta Metallurgica et Materialia 42 (2) (1994) 475–487. doi:10.1016/0956-7151(94)90502-9.

[20] J. S. Stolken, A. G. Evans, A microbend test method for measuring the plasticity length scale, Acta Materialia 46 (14) (1998) 5109–5115. doi:10.1016/S1359-6454(98)00153-0.

[21] D. Lam, F. Yang, A. Chong, J. Wang, P. Tong, Experiments and theory in strain gradient elasticity, Journal of the Mechanics and Physics of Solids 51 (8) (2003) 1477 – 1508. doi:http://dx.doi.org/10.1016/S0022-5096(03)00053-X.

[22] A. C. Eringen, Nonlocal polar elastic continua, International Journal of Engineering Science 10 (1) (1972) 1–16. doi:10.1016/0020-7225(72)90070-5.

[23] N. A. Fleck, J. W. Hutchinson, A phenomenological theory for strain gradient effects in plasticity, Journal of the Mechanics and Physics of Solids 41 (12) (1993) 1825–1857. doi:10.1016/0022-5096(93)90072-N.

[24] F. Yang, A. C. M. Chong, D. C. C. Lam, P. Tong, Couple stress based strain gradient theory for elasticity, International Journal of Solids and Structures 39 (10) (2002) 2731–2743. doi:10.1016/S0020-7683(02)00152-X.

[25] R. D. Mindlin, H. F. Tiersten, Effects of couple-stresses in linear elasticity, Archive for Rational Mechanics and Analysis 11 (1) (1962) 415–448. doi:10.1007/BF00253946.

[26] R. D. Mindlin, Second gradient of strain and surface-tension in linear elasticity, International Journal of Solids and Structures 1 (4) (1965) 417–438. doi:10.1016/0020-7683(65)90006-5.

[27] R. Ansari, R. Gholami, M. Faghih Shojaei, V. Mohammadi, S. Sahmani, Size-dependent bending, buckling and free vibration of functionally graded timoshenko microbeams based on the most general strain gradient theory, Composite Structures 100 (2013) 385–397. doi:10.1016/j.compstruct.2012.12.048.

[28] S. K. Park, X.-L. Gao, Variational formulation of a modified couple stress theory and its application to a simple shear problem, Zeitschrift fr angewandte Mathematik und Physik 59 (5) (2007) 904–917. doi:10.1007/s00033-006-6073-8.

[29] S. K. Park, X.-L. Gao, BernoulliEuler beam model based on a modified couple stress theory, Journal of Micromechanics and Microengineering 16 (11) (2006) 2355. doi:10.1088/0960-1317/16/11/015.
[30] W. Xia, L. Wang, L. Yin, Nonlinear non-classical microscale beams: Static bending, postbuckling and free vibration, International Journal of Engineering Science 48 (12) (2010) 2044–2053. doi:10.1016/j.ijengsci.2010.04.010.
[31] L.-L. Ke, Y.-S. Wang, Size effect on dynamic stability of functionally graded microbeams based on a modified couple stress theory, Composite Structures 93 (2) (2011) 342–350. doi:10.1016/j.compstruct.2010.09.008.
[32] C. M. C. Roque, D. S. Fidalgo, A. J. M. Ferreira, J. N. Reddy, A study of a microstructure-dependent composite laminated Timoshenko beam using a modified couple stress theory and a meshless method, Composite Structures 96 (2013) 532–537. doi:10.1016/j.compstruct.2012.09.011.
[33] H.-T. Thai, T. P. Vo, T.-K. Nguyen, J. Lee, Size-dependent behavior of functionally graded sandwich microbeams based on the modified couple stress theory, Composite Structures 123 (2015) 337–349. doi:10.1016/j.compstruct.2014.11.065.
[34] M. Salamat-talab, A. Nateghi, J. Torabi, Static and dynamic analysis of third-order shear deformation FG micro beam based on modified couple stress theory, International Journal of Mechanical Sciences 57 (1) (2012) 63–73. doi:10.1016/j.ijmecsci.2012.02.004.
[35] G. C. Tsiatas, A new Kirchhoff plate model based on a modified couple stress theory, International Journal of Solids and Structures 46 (13) (2009) 2757–2764. doi:10.1016/j.ijsolstr.2009.03.004.
[36] L. Yin, Q. Qian, L. Wang, W. Xia, Vibration analysis of microscale plates based on modified couple stress theory, Acta Mechanica Solida Sinica 23 (5) (2010) 386 – 393. doi:http://dx.doi.org/10.1016/S0894-9166(10)60040-7.
[37] H. M. Ma, X.-L. Gao, J. N. Reddy, A non-classical Mindlin plate model based on a modified couple stress theory, Acta Mechanica 220 (1-4) (2011) 217–235. doi:10.1007/s00707-011-0480-4.
[38] M. Simsek, T. Kocaturk, S. D. Akbas, Static bending of a functionally graded microscale Timoshenko beam based on the modified couple stress theory, Composite Structures 95 (2013) 740–747. doi:10.1016/j.compstruct.2012.08.036.
[39] A. Nateghi, M. Salamat-talab, J. Rezapour, B. Daneshian, Size dependent buckling analysis of functionally graded micro beams based on modified couple stress theory, Applied Mathematical Modelling 36 (10) (2012) 4971–4987. doi:10.1016/j.apm.2011.12.035.
[40] H.-T. Thai, S.-E. Kim, A size-dependent functionally graded reddy plate model based on a modified couple stress theory, Composites Part B: Engineering 45 (1) (2013) 1636 – 1645. doi:http://dx.doi.org/10.1016/j.compositesb.2012.09.065.
[41] H.-T. Thai, D.-H. Choi, Size-dependent functionally graded kirchhoff and mindlin plate models based on a modified couple stress theory, Composite Structures 95 (2013) 142 – 153. doi:http://dx.doi.org/10.1016/j.compstruct.2012.08.023.
[42] H.-T. Thai, T. P. Vo, A size-dependent functionally graded sinusoidal plate model based on a modified couple stress theory, Composite Structures 96 (2013) 376–383. doi:10.1016/j.compstruct.2012.09.025.
[43] L.-L. Ke, Y.-S. Wang, J. Yang, S. Kitipornchai, Free vibration of size-dependent Mindlin microplates based on the modified couple stress theory, Journal of Sound and Vibration 331 (1) (2012) 94–106. doi:10.1016/j.jsv.2011.08.020.
[44] L.-L. Ke, J. Yang, S. Kitipornchai, M. A. Bradford, Bending, buckling and vibration of size-dependent functionally graded annular microplates, Composite Structures 94 (11) (2012) 3250–3257. doi:10.1016/j.compstruct.2012.04.037.
[45] L. He, J. Lou, E. Zhang, Y. Wang, Y. Bai, A size-dependent four variable refined plate model for functionally graded microplates based on modified couple stress theory, Composite Structures 130 (2015) 107 – 115. doi:http://dx.doi.org/10.1016/j.compstruct.2015.04.033.
[46] J. N. Reddy, J. Kim, A nonlinear modified couple stress-based third-order theory of functionally graded plates, Composite Structures 94 (3) (2012) 1128–1143. doi:10.1016/j.compstruct.2011.10.006.
[47] J. N. Reddy, J. Berry, Nonlinear theories of axisymmetric bending of functionally graded circular

plates with modified couple stress, Composite Structures 94 (12) (2012) 3664–3668. doi:10.1016/j.compstruct.2012.04.019.

[48] J. Kim, J. N. Reddy, A general third-order theory of functionally graded plates with modified couple stress effect and the von karman nonlinearity: theory and finite element analysis, Acta Mechanica 226 (9) (2015) 2973–2998. doi:10.1007/s00707-015-1370-y.

[49] J. N. Reddy, J. Romanoff, J. A. Loya, Nonlinear Finite Element Analysis of Functionally Graded Circular Plates with Modified Couple Stress Theory, European Journal of Mechanics - A/Solidsdoi:10.1016/j.euromechsol.2015.11.001.

[50] L. Della Croce, P. Venini, Finite elements for functionally graded ReissnerMindlin plates, Computer Methods in Applied Mechanics and Engineering 193 (911) (2004) 705–725. doi:10.1016/j.cma.2003.09.014.

[51] H. Nguyen-Xuan, G. R. Liu, C. Thai-Hoang, T. Nguyen-Thoi, An edge-based smoothed finite element method (ES-FEM) with stabilized discrete shear gap technique for analysis of ReissnerMindlin plates, Computer Methods in Applied Mechanics and Engineering 199 (912) (2010) 471–489. doi:10.1016/j.cma.2009.09.001.

[52] B. Zhang, Y. He, D. Liu, Z. Gan, L. Shen, A non-classical Mindlin plate finite element based on a modified couple stress theory, European Journal of Mechanics - A/Solids 42 (2013) 63–80. doi:10.1016/j.euromechsol.2013.04.005.

[53] J. N. Reddy, A Simple Higher-Order Theory for Laminated Composite Plates, Journal of Applied Mechanics 51 (4) (1984) 745–752. doi:10.1115/1.3167719.

[54] H. Nguyen-Xuan, C. H. Thai, T. Nguyen-Thoi, Isogeometric finite element analysis of composite sandwich plates using a higher order shear deformation theory, Composites Part B: Engineering 55 (2013) 558–574. doi:10.1016/j.compositesb.2013.06.044.

[55] H. Arya, R. P. Shimpi, N. K. Naik, A zigzag model for laminated composite beams, Composite Structures 56 (1) (2002) 21–24. doi:10.1016/S0263-8223(01)00178-7.

[56] N. R. Senthilnathan, S. P. Lim, K. H. Lee, S. T. Chow, Buckling of Shear-Deformable Plates, AIAA Journal 25 (9) (1987) 1268–1271. doi:10.2514/3.48742.

[57] R. P. Shimpi, Refined plate theory and its variants, AIAA journal 40 (1) (2002) 137–146.

[58] R. P. Shimpi, H. G. Patel, A two variable refined plate theory for orthotropic plate analysis, International Journal of Solids and Structures 43 (2223) (2006) 6783–6799. doi:10.1016/j.ijsolstr.2006.02.007.

[59] R. P. Shimpi, H. G. Patel, Free vibrations of plate using two variable refined plate theory, Journal of Sound and Vibration 296 (45) (2006) 979–999. doi:10.1016/j.jsv.2006.03.030.

[60] C. A. Shankara, N. G. R. Iyengar, A C0 element for the free vibration analysis of laminated composite plates, Journal of Sound and Vibration 191 (5) (1996) 721–738. doi:10.1006/jsvi.1996.0152.

[61] T. Hughes, J. Cottrell, Y. Bazilevs, Isogeometric analysis: Cad, finite elements, nurbs, exact geometry and mesh refinement, Computer Methods in Applied Mechanics and Engineering 194 (3941) (2005) 4135 – 4195. doi:http://dx.doi.org/10.1016/j.cma.2004.10.008.

[62] J. A. Cottrell, T. J. R. Hughes, Y. Bazilevs, Isogeometric Analysis: Toward Integration of CAD and FEA, 1st Edition, Wiley Publishing, 2009.

[63] H. Nguyen-Xuan, L. V. Tran, C. H. Thai, S. Kulasegaram, S. Bordas, Isogeometric analysis of functionally graded plates using a refined plate theory, Composites Part B: Engineering 64 (2014) 222 – 234. doi:http://dx.doi.org/10.1016/j.compositesb.2014.04.001.

[64] A. V. Vuong, C. Heinrich, B. Simeon, ISOGAT: A 2d tutorial MATLAB code for Isogeometric Analysis, Computer Aided Geometric Design 27 (8) (2010) 644–655. doi:10.1016/j.cagd.2010.06.006.

[65] C. de Falco, A. Reali, R. Vzquez, GeoPDEs: A research tool for Isogeometric Analysis of PDEs, Advances in Engineering Software 42 (12) (2011) 1020–1034. doi:10.1016/j.advengsoft.2011.06.010.

[66] V. P. Nguyen, C. Anitescu, S. P. A. Bordas, T. Rabczuk, Isogeometric analysis: An overview and computer implementation aspects, Mathematics and Computers in Simulation 117 (2015) 89–116. doi:10.1016/j.matcom.2015.05.008.

[67] C. H. Thai, A. J. M. Ferreira, E. Carrera, H. Nguyen-Xuan, Isogeometric analysis of laminated composite and sandwich plates using a layerwise deformation theory, Composite Structures 104 (2013) 196–214. doi:10.1016/j.compstruct.2013.04.002.

[68] L. Beiro da Veiga, A. Buffa, C. Lovadina, M. Martinelli, G. Sangalli, An isogeometric method for the ReissnerMindlin plate bending problem, Computer Methods in Applied Mechanics and Engineering 209212 (2012) 45–53. doi:10.1016/j.cma.2011.10.009.

[69] C. H. Thai, H. Nguyen-Xuan, N. Nguyen-Thanh, T.-H. Le, T. Nguyen-Thoi, T. Rabczuk, Static, free vibration, and buckling analysis of laminated composite Reissner–Mindlin plates using NURBS-based isogeometric approach, International Journal for Numerical Methods in Engineering 91 (6) (2012) 571–603. doi:10.1002/nme.4282.

[70] N. Valizadeh, S. Natarajan, O. A. Gonzalez-Estrada, T. Rabczuk, T. Q. Bui, S. P. A. Bordas, NURBS-based finite element analysis of functionally graded plates: Static bending, vibration, buckling and flutter, Composite Structures 99 (2013) 309–326. doi:10.1016/j.compstruct.2012.11.008.

[71] L. V. Tran, C. H. Thai, H. Nguyen-Xuan, An isogeometric finite element formulation for thermal buckling analysis of functionally graded plates, Finite Elements in Analysis and Design 73 (2013) 65–76. doi:10.1016/j.finel.2013.05.003.

[72] C. H. Thai, A. J. M. Ferreira, S. P. A. Bordas, T. Rabczuk, H. Nguyen-Xuan, Isogeometric analysis of laminated composite and sandwich plates using a new inverse trigonometric shear deformation theory, European Journal of Mechanics - A/Solids 43 (2014) 89–108. doi:10.1016/j.euromechsol.2013.09.001.

[73] C. H. Thai, H. Nguyen-Xuan, S. P. A. Bordas, N. Nguyen-Thanh, T. Rabczuk, Isogeometric Analysis of Laminated Composite Plates Using the Higher-Order Shear Deformation Theory, Mechanics of Advanced Materials and Structures 22 (6) (2015) 451–469. doi:10.1080/15376494.2013.779050.

[74] J. Kiendl, K. U. Bletzinger, J. Linhard, R. Wchner, Isogeometric shell analysis with KirchhoffLove elements, Computer Methods in Applied Mechanics and Engineering 198 (4952) (2009) 3902–3914. doi:10.1016/j.cma.2009.08.013.

[75] N. Nguyen-Thanh, J. Kiendl, H. Nguyen-Xuan, R. Wchner, K. U. Bletzinger, Y. Bazilevs, T. Rabczuk, Rotation free isogeometric thin shell analysis using PHT-splines, Computer Methods in Applied Mechanics and Engineering 200 (4748) (2011) 3410–3424. doi:10.1016/j.cma.2011.08.014.

[76] N. Nguyen-Thanh, N. Valizadeh, M. N. Nguyen, H. Nguyen-Xuan, X. Zhuang, P. Areias, G. Zi, Y. Bazilevs, L. De Lorenzis, T. Rabczuk, An extended isogeometric thin shell analysis based on KirchhoffLove theory, Computer Methods in Applied Mechanics and Engineering 284 (2015) 265–291. doi:10.1016/j.cma.2014.08.025.

[77] S. S. Vel, R. C. Batra, Exact Solution for Thermoelastic Deformations of Functionally Graded Thick Rectangular Plates, AIAA Journal 40 (7) (2002) 1421–1433. doi:10.2514/2.1805.

[78] L. F. Qian, R. C. Batra, L. M. Chen, Static and dynamic deformations of thick functionally graded elastic plates by using higher-order shear and normal deformable plate theory and meshless local PetrovGalerkin method, Composites Part B: Engineering 35 (68) (2004) 685–697. doi:10.1016/j.compositesb.2004.02.004.

[79] T. Mori, K. Tanaka, Average stress in matrix and average elastic energy of materials with misfitting inclusions, Acta Metallurgica 21 (5) (1973) 571–574. doi:10.1016/0001-6160(73)90064-3.

[80] Y. Kiani, M. R. Eslami, Thermal Postbuckling of Imperfect Circular Functionally Graded Material Plates: Examination of Voigt, MoriTanaka, and Self-Consistent Schemes, Journal of Pressure Vessel Technology 137 (2) (2014) 021201–021201. doi:10.1115/1.4026993.

[81] E. Carrera, S. Brischetto, M. Cinefra, M. Soave, Effects of thickness stretching in functionally graded plates and shells, Composites Part B: Engineering 42 (2) (2011) 123 – 133. doi:http://dx.doi.org/10.1016/j.compositesb.2010.10.005.

[82] J. L. Mantari, C. Guedes Soares, A novel higher-order shear deformation theory with stretching effect for functionally graded plates, Composites Part B: Engineering 45 (1) (2013) 268–281. doi:10.1016/j.compositesb.2012.05.036.

[83] C. H. Thai, A. M. Zenkour, M. Abdel Wahab, H. Nguyen-Xuan, A simple four-unknown shear and nor-

mal deformations theory for functionally graded isotropic and sandwich plates based on isogeometric analysis, Composite Structures 139 (2016) 77–95. doi:10.1016/j.compstruct.2015.11.066.

[84] A. M. Zenkour, A simple four-unknown refined theory for bending analysis of functionally graded plates, Applied Mathematical Modelling 37 (2013) 9041 – 9051. doi:http://dx.doi.org/10.1016/j.apm.2013.04.022.

[85] A. M. Zenkour, Bending analysis of functionally graded sandwich plates using a simple four-unknown shear and normal deformations theory, Journal of Sandwich Structures and Materials 15 (6) (2013) 629–656. doi:10.1177/1099636213498886.

[86] A. Neves, A. Ferreira, E. Carrera, C. Roque, M. Cinefra, R. Jorge, C. Soares, A quasi-3d sinusoidal shear deformation theory for the static and free vibration analysis of functionally graded plates, Composites Part B: Engineering 43 (2) (2012) 711 – 725. doi:http://dx.doi.org/10.1016/j.compositesb.2011.08.009.

[87] J. L. Mantari, C. Guedes Soares, Generalized hybrid quasi-3d shear deformation theory for the static analysis of advanced composite plates, Composite Structures 94 (8) (2012) 2561–2575. doi:10.1016/j.compstruct.2012.02.019.

[88] H.-T. Thai, S.-E. Kim, A simple quasi-3d sinusoidal shear deformation theory for functionally graded plates, Composite Structures 99 (2013) 172–180. doi:10.1016/j.compstruct.2012.11.030.

[89] T. N. Nguyen, C. H. Thai, H. Nguyen-Xuan, On the general framework of high order shear deformation theories for laminated composite plate structures: A novel unified approach, International Journal of Mechanical Sciences 110 (2016) 242–255. doi:10.1016/j.ijmecsci.2016.01.012.

[90] J. N. Reddy, Theory and Analysis of Elastic Plates and Shells, 2nd Edition, CRC Press, 2006.

[91] N.-T. Nguyen, D. Hui, J. Lee, H. Nguyen-Xuan, An efficient computational approach for size-dependent analysis of functionally graded nanoplates, Computer Methods in Applied Mechanics and Engineering 297 (2015) 191 – 218. doi:http://dx.doi.org/10.1016/j.cma.2015.07.021.

[92] K.-J. Bathe, A. Iosilevich, D. Chapelle, An evaluation of the MITC shell elements, Computers & Structures 75 (1) (2000) 1–30. doi:10.1016/S0045-7949(99)00214-X.

[93] L. V. Tran, T. Nguyen-Thoi, C. H. Thai, H. Nguyen-Xuan, An Edge-Based Smoothed Discrete Shear Gap Method Using the C0-Type Higher-Order Shear Deformation Theory for Analysis of Laminated Composite Plates, Mechanics of Advanced Materials and Structures 22 (4) (2015) 248–268. doi:10.1080/15376494.2012.736055.

[94] F. Auricchio, L. B. da Veiga, A. Buffa, C. Lovadina, A. Reali, G. Sangalli, A fully locking-free isogeometric approach for plane linear elasticity problems: A stream function formulation, Computer Methods in Applied Mechanics and Engineering 197 (14) (2007) 160 – 172. doi:http://dx.doi.org/10.1016/j.cma.2007.07.005.

[95] M. Mohammadi, M. Ghayour, A. Farajpour, Free transverse vibration analysis of circular and annular graphene sheets with various boundary conditions using the nonlocal continuum plate model, Composites Part B: Engineering 45 (1) (2013) 32 – 42. doi:http://dx.doi.org/10.1016/j.compositesb.2012.09.011.

[96] L. Ma, T. Wang, Relationships between axisymmetric bending and buckling solutions of {FGM} circular plates based on third-order plate theory and classical plate theory, International Journal of Solids and Structures 41 (1) (2004) 85 – 101. doi:http://dx.doi.org/10.1016/j.ijsolstr.2003.09.008.

[97] A. Saidi, A. Rasouli, S. Sahraee, Axisymmetric bending and buckling analysis of thick functionally graded circular plates using unconstrained third-order shear deformation plate theory, Composite Structures 89 (1) (2009) 110 – 119. doi:http://dx.doi.org/10.1016/j.compstruct.2008.07.003.

[98] L. V. Tran, A. Ferreira, H. Nguyen-Xuan, Isogeometric analysis of functionally graded plates using higher-order shear deformation theory, Composites Part B: Engineering 51 (2013) 368 – 383. doi:http://dx.doi.org/10.1016/j.compositesb.2013.02.045.

[99] J. L. Mantari, C. G. Soares, A quasi-3d tangential shear deformation theory with four unknowns for functionally graded plates, Acta Mechanica 226 (3) (2014) 625–642. doi:10.1007/s00707-014-1192-3.

[100] S. Akavci, A. Tanrikulu, Static and free vibration analysis of functionally graded plates based on a new quasi-3d and 2d shear deformation theories, Composites Part B: Engineering 83 (2015) 203 – 215. doi:http://dx.doi.org/10.1016/j.compositesb.2015.08.043.

[101] A. M. Zenkour, Generalized shear deformation theory for bending analysis of functionally graded plates, Applied Mathematical Modelling 30 (1) (2006) 67 – 84. doi:http://dx.doi.org/10.1016/j.apm.2005.03.009.

[102] S. S. Vel, R. Batra, Three-dimensional exact solution for the vibration of functionally graded rectangular plates, Journal of Sound and Vibration 272 (35) (2004) 703 – 730. doi:http://dx.doi.org/10.1016/S0022-460X(03)00412-7.

[103] H. Matsunaga, Free vibration and stability of functionally graded plates according to a 2-d higher-order deformation theory, Composite Structures 82 (4) (2008) 499 – 512. doi:http://dx.doi.org/10.1016/j.compstruct.2007.01.030.

[104] Z. Belabed, M. S. A. Houari, A. Tounsi, S. Mahmoud, O. A. Bg, An efficient and simple higher order shear and normal deformation theory for functionally graded material (fgm) plates, Composites Part B: Engineering 60 (2014) 274 – 283. doi:http://dx.doi.org/10.1016/j.compositesb.2013.12.057.

[105] F. Alijani, M. Amabili, Effect of thickness deformation on large-amplitude vibrations of functionally graded rectangular plates, Composite Structures 113 (2014) 89 – 107. doi:http://dx.doi.org/10.1016/j.compstruct.2014.03.006.

Table 1: Various forms of distribution function used for HSDT, RPT, and quasi-3D theories

Theory	ε_z	$f(z)$	ϕ_z
HSDT [53]	$=0$	$z-\frac{4}{3}\frac{z^3}{h^2}$	-
RPT [63]	$=0$	$\arctan\left(\sin\left(\frac{\pi}{h}z\right)\right)$	-
Quasi-3D [84]	$\neq 0$	$h\sinh\left(\frac{z}{h}\right)-\frac{4z^3}{3h^2}\cosh\left(\frac{1}{2}\right)$	$\frac{1}{12}f'(z)$
Quasi-3D [88]	$\neq 0$	$\frac{h}{\pi}\sin\left(\frac{\pi z}{h}\right)-z$	$f'(z)+1$
Quasi-3D [91]	$\neq 0$	$\frac{\pi}{h}z-\frac{9\pi}{5h^3}z^3+\frac{28\pi}{25h^5}z^5$	$\frac{1}{8}f'(z)$
Present RPT	$=0$	$-8z+\frac{10z^3}{h^2}+\frac{6z^5}{5h^4}+\frac{8z^7}{7h^6}$	-
Present quasi-3D	$\neq 0$	$-8z+\frac{10z^3}{h^2}+\frac{6z^5}{5h^4}+\frac{8z^7}{7h^6}$	$\frac{3}{20}f'(z)$

Table 2: Material properties of FG plates

Property	Material			
	Al	Al_2O_3	ZrO_2-1	ZrO_2-2
E (GPa)	70	380	200	151
ν	0.3	0.3	0.3	0.3
ρ (kg/m^3)	2707	3800	3000	3000

Table 3: Convergence of non-dimensional central deflections $\bar{w} = \dfrac{10Eh^3}{q_0 L^4} w\,(a/2, a/2, 0)$ of SSSS homogeneous square plate subjected to sinusoidally distributed load ($a/h = 20$)

ℓ/h	p	Element Mesh								Analytical [40]
		3×3	5×5	7×7	9×9	11×11	13×13	15×15	17×17	
0										0.2842
	2	0.2734	0.2799	0.2819	0.2828	0.2833	0.2835	0.2837	0.2838	
	3	0.2823	0.2841	0.2842	0.2842	0.2842	0.2842	0.2842	0.2842	
	4	0.2843	0.2842	0.2842	0.2842	0.2842	0.2842	0.2842	0.2842	
0.2										0.2430
	2	0.2346	0.2397	0.2413	0.2420	0.2424	0.2426	0.2427	0.2428	
	3	0.2415	0.2430	0.2431	0.2431	0.2431	0.2431	0.2431	0.2431	
	4	0.2432	0.2431	0.2431	0.2431	0.2431	0.2431	0.2431	0.2431	
0.6										0.1124
	2	0.1098	0.1115	0.1121	0.1123	0.1125	0.1125	0.1126	0.1126	
	3	0.1120	0.1127	0.1127	0.1127	0.1127	0.1127	0.1127	0.1127	
	4	0.1127	0.1127	0.1127	0.1127	0.1127	0.1127	0.1127	0.1127	
1										0.0542
	2	0.0532	0.0539	0.0541	0.0542	0.0543	0.0543	0.0543	0.0543	
	3	0.0541	0.0544	0.0544	0.0544	0.0544	0.0544	0.0544	0.0544	
	4	0.0544	0.0544	0.0544	0.0544	0.0544	0.1127	0.1127	0.1127	

Table 4: Comparison of non-dimensional deflections $\bar{w} = \dfrac{10E_c h^3}{q_0 L^4} w\,(a/2, b/2, 0)$ of SSSS Al/Al_2O_3 square plates (rule of mixtures scheme)

n	Theory	$\varepsilon_z = 0$			$\varepsilon_z \neq 0$		
		$a/h = 4$	$a/h = 10$	$a/h = 100$	$a/h = 4$	$a/h = 10$	$a/h = 100$
Sinusoidally distributed load							
1	Zenkour [84]	-	-	-	0.6828	0.5592	0.5624
	Neves et al. [86]	-	-	-	0.6997	0.5845	0.5624
	Mantari and Soares [99]	-	-	-	0.693	0.569	0.545
	Carrera et al. [81]	0.7289	0.5890	0.5625	0.7171	0.5875	0.5625
	Akavci and Tanrikulu [100]	0.7282	0.5889	0.5625	0.6908	0.5691	0.5457
	IGA-Reddy [53]	0.7284	0.5889	0.5625	-	-	-
	IGA-Zenkour [84]	0.7284	0.5889	0.5625	0.6828	0.5592	0.5459
	IGA-Nguyen et al. [91]	0.7275	0.5888	0.5625	0.6880	0.5640	0.5422
	IGA-Present†	0.7284	0.5889	0.5625	0.6935	0.5691	0.5460
4	Zenkour [84]	-	-	-	1.1001	0.8404	0.7933
	Neves et al. [86]	-	-	-	1.1178	0.8750	0.8286
	Mantari and Soares [99]	-	-	-	1.085	0.838	0.793
	Carrera et al. [81]	1.1673	0.8828	0.8286	1.1585	0.8821	0.8286
	Akavci and Tanrikulu [100]	1.1613	0.8818	0.8287	1.0983	0.8417	0.7925
	IGA-Reddy [53]	1.1598	0.8815	0.8287	-	-	-
	IGA-Zenkour [84]	1.1599	0.8815	0.8287	1.1001	0.8404	0.7933
	IGA-Nguyen et al. [91]	1.1625	0.8820	0.8287	1.0931	0.8363	0.7875
	IGA-Present†	1.1590	0.8813	0.8287	1.0868	0.8392	0.7933
10	Zenkour [84]	-	-	-	1.3391	0.9806	0.9140
	Neves et al. [86]	-	-	-	1.3490	0.8750	0.8286
	Mantari and Soares [99]	-	-	-	1.308	0.972	0.911
	Carrera et al. [81]	1.3925	1.0090	0.9361	1.3745	1.0072	0.9361
	Akavci and Tanrikulu [100]	1.3917	1.0089	0.9362	1.3352	0.9818	0.9141
	IGA-Reddy [53]	1.3908	1.0087	0.9362	-	-	-
	IGA-Zenkour [84]	1.3908	1.0087	0.9362	1.3391	0.9806	0.9140
	IGA-Nguyen et al. [91]	1.3914	1.0089	0.9362	1.3260	0.9760	0.9096
	IGA-Present†	1.3902	1.0086	0.9362	1.3116	0.9748	0.9132
Uniformly distributed load							
1	Zenkour [101]	-	0.9287	-	-	-	-
	Akavci and Tanrikulu [100]	-	0.9288	-	-	0.8977	-
	IGA-Reddy [53]	1.1319	0.9288	0.8904	-	-	-
	IGA-Zenkour [84]	1.1319	0.9288	0.8904	1.0611	0.8822	0.8641
	IGA-Nguyen et al. [91]	1.1308	0.9286	0.8904	1.0701	0.8898	0.8582
	IGA-Present†	1.1319	0.9288	0.8904	1.0788	0.8978	0.8642
4	Zenkour [101]	-	1.3890	-	-	-	-
	Akavci and Tanrikulu [100]	-	1.3888	-	-	1.3259	-
	IGA-Reddy [53]	1.7941	1.3884	1.3116	-	-	-
	IGA-Zenkour [84]	1.7942	1.3884	1.3116	1.7020	1.3238	1.2556
	IGA-Nguyen et al. [91]	1.7983	1.3892	1.3116	1.6919	1.3174	1.2464
	IGA-Present†	1.7928	1.3882	1.3116	1.6827	1.3223	1.2556
10	Zenkour [101]	-	1.5876	-	-	-	-
	Akavci and Tanrikulu [100]	-	1.5875	-	-	1.5453	-
	IGA-Reddy [53]	2.1442	1.5872	1.4818	-	-	-
	IGA-Zenkour [84]	2.1442	1.5872	1.4818	2.0656	1.5433	1.4466
	IGA-Nguyen et al. [91]	2.1454	1.5876	1.4818	2.0466	1.5362	1.4397
	IGA-Present†	2.1432	1.5870	1.4818	2.0244	1.5347	1.4454

†Proposed RPT and quasi-3D models are used for the case of $\varepsilon_z = 0$ and $\varepsilon_z \neq 0$, respectively.

Table 5: Non-dimensional deflection $\bar{w} = \dfrac{10E_c h^3}{q_0 L^4} w\left(a/2, b/2, 0\right)$ of SSSS Al/Al_2O_3 square microplates subjected to sinusoidally distributed load (rule of mixtures scheme)

a/h	ℓ/h	$n=0$			$n=1$			$n=10$		
		RPT	Quasi-3D	TSDT[40]	RPT	Quasi-3D	TSDT[40]	RPT	Quasi-3D	TSDT[40]
5	0	0.3433	0.3360	0.3433	0.6688	0.6401	0.6688	1.2271	1.1663	1.2276
	0.2	0.2898	0.2853	0.2875	0.5505	0.5321	0.5468	1.0400	1.0019	1.0247
	0.4	0.1975	0.1965	0.1934	0.3601	0.3537	0.3535	0.7140	0.7043	0.6908
	0.6	0.1292	0.1296	0.1251	0.2288	0.2274	0.2224	0.4694	0.4711	0.4514
	0.8	0.0871	0.0879	0.0838	0.1517	0.1520	0.1464	0.3174	0.3220	0.3052
	1	0.0614	0.0623	0.0588	0.1060	0.1069	0.1017	0.2242	0.2289	0.2158
20	0	0.2842	0.2836	0.2842	0.5689	0.5516	0.5689	0.9537	0.9280	0.9538
	0.2	0.2431	0.2427	0.2430	0.4739	0.4619	0.4737	0.8313	0.8120	0.8303
	0.4	0.1695	0.1694	0.1693	0.3157	0.3105	0.3153	0.6001	0.5906	0.5986
	0.6	0.1127	0.1127	0.1124	0.2029	0.2008	0.2025	0.4102	0.4061	0.4090
	0.8	0.0767	0.0768	0.0765	0.1352	0.1343	0.1349	0.2842	0.2825	0.2834
	1	0.0544	0.0544	0.0542	0.0947	0.0943	0.0944	0.2038	0.2031	0.2033
100	0	0.2804	0.2803	0.2804	0.5625	0.5460	0.5625	0.9362	0.9132	0.9362
	0.2	0.2401	0.2400	0.2401	0.4689	0.4574	0.4689	0.8176	0.8001	0.8176
	0.4	0.1677	0.1677	0.1677	0.3128	0.3076	0.3128	0.5925	0.5833	0.5925
	0.6	0.1116	0.1116	0.1116	0.2012	0.1990	0.2011	0.4062	0.4018	0.4061
	0.8	0.0760	0.0760	0.0760	0.1341	0.1332	0.1341	0.2820	0.2799	0.2820
	1	0.0539	0.0539	0.0539	0.0939	0.0934	0.0939	0.2024	0.2014	0.2024

Table 6: Non-dimensional deflection $\bar{w} = \dfrac{10E_c h^3}{q_0 L^4} w\,(a/2, b/2, 0)$ of CCCC Al/Al_2O_3 square microplates (rule of mixtures scheme)

a/h	ℓ/h	$n=0$			$n=1$			$n=10$		
		RPT	Quasi-3D	IGA-Reddy	RPT	Quasi-3D	IGA-Reddy	RPT	Quasi-3D	IGA-Reddy
Sinusoidally distributed load										
5	0	0.1601	0.1359	0.1601	0.3021	0.2554	0.3020	0.6111	0.4740	0.6113
	0.2	0.1378	0.1197	0.1377	0.2555	0.2214	0.2554	0.5178	0.4199	0.5183
	0.4	0.0974	0.0883	0.0973	0.1751	0.1586	0.1751	0.3568	0.3132	0.3575
	0.6	0.0655	0.0616	0.0655	0.1151	0.1081	0.1151	0.2358	0.2204	0.2364
	0.8	0.0450	0.0435	0.0449	0.0779	0.0752	0.0779	0.1602	0.1559	0.1606
	1	0.0321	0.0316	0.0320	0.0551	0.0542	0.0551	0.1136	0.1134	0.1139
20	0	0.1035	0.0950	0.1035	0.2065	0.1863	0.2065	0.3505	0.3150	0.3505
	0.2	0.0919	0.0849	0.0919	0.1797	0.1638	0.1797	0.3150	0.2857	0.3151
	0.4	0.0688	0.0645	0.0688	0.1294	0.1204	0.1294	0.2419	0.2237	0.2420
	0.6	0.0485	0.0462	0.0485	0.0882	0.0837	0.0882	0.1746	0.1647	0.1747
	0.8	0.0343	0.0331	0.0343	0.0611	0.0587	0.0611	0.1258	0.1204	0.1258
	1	0.0250	0.0243	0.0250	0.0438	0.0425	0.0438	0.0926	0.0896	0.0926
100	0	0.0999	0.0955	0.0999	0.2003	0.1872	0.2003	0.3336	0.3131	0.3336
	0.2	0.0889	0.0853	0.0889	0.1746	0.1643	0.1746	0.3013	0.2842	0.3013
	0.4	0.0668	0.0646	0.0668	0.1262	0.1204	0.1262	0.2336	0.2228	0.2336
	0.6	0.0473	0.0461	0.0473	0.0863	0.0835	0.0863	0.1701	0.1640	0.1701
	0.8	0.0336	0.0329	0.0336	0.0599	0.0584	0.0599	0.1232	0.1199	0.1233
	1	0.0244	0.0241	0.0244	0.0430	0.0422	0.0430	0.0910	0.0891	0.0910
Uniformly distributed load										
5	0	0.2239	0.1860	0.2238	0.4220	0.3500	0.4219	0.8557	0.6408	0.8559
	0.2	0.1924	0.1641	0.1924	0.3566	0.3040	0.3565	0.7233	0.5701	0.7239
	0.4	0.1358	0.1215	0.1358	0.2443	0.2186	0.2442	0.4976	0.4286	0.4985
	0.6	0.0914	0.0851	0.0913	0.1606	0.1495	0.1605	0.3288	0.3034	0.3295
	0.8	0.0627	0.0602	0.0627	0.1087	0.1041	0.1087	0.2234	0.2154	0.2239
	1	0.0447	0.0439	0.0447	0.0769	0.0752	0.0769	0.1584	0.1570	0.1588
20	0	0.1436	0.1300	0.1436	0.2864	0.2553	0.2864	0.4863	0.4307	0.4863
	0.2	0.1275	0.1164	0.1275	0.2493	0.2248	0.2493	0.4372	0.3912	0.4373
	0.4	0.0956	0.0887	0.0956	0.1797	0.1657	0.1797	0.3360	0.3072	0.3361
	0.6	0.0674	0.0637	0.0674	0.1227	0.1156	0.1227	0.2428	0.2269	0.2429
	0.8	0.0478	0.0457	0.0478	0.0850	0.0813	0.0850	0.1750	0.1664	0.1751
	1	0.0348	0.0336	0.0348	0.0610	0.0589	0.0610	0.1289	0.1240	0.1289
100	0	0.1384	0.1314	0.1384	0.2775	0.2577	0.2775	0.4622	0.4310	0.4622
	0.2	0.1232	0.1174	0.1232	0.2421	0.2265	0.2421	0.4176	0.3915	0.4176
	0.4	0.0927	0.0891	0.0927	0.1751	0.1664	0.1751	0.3242	0.3075	0.3242
	0.6	0.0657	0.0637	0.0657	0.1199	0.1155	0.1199	0.2363	0.2268	0.2363
	0.8	0.0467	0.0456	0.0467	0.0833	0.0810	0.0833	0.1713	0.1661	0.1713
	1	0.0340	0.0334	0.0340	0.0598	0.0586	0.0598	0.1266	0.1236	0.1266

Table 7: Comparison of non-dimensional natural frequencies $\bar{\omega} = \omega \frac{a^2}{h}\sqrt{\frac{\rho_m}{E_m}}$ of SSSS Al/ZrO_2-1 plates (Mori-Tanaka scheme)

Theory	$n = 1$			$a/h = 5$		
	$a/h = 5$	$a/h = 10$	$a/h = 20$	$n = 2$	$n = 3$	$n = 5$
Vel and Batra [102]	5.4806	5.9609	6.1076	5.4923	5.5285	5.5632
Matsunaga [103]	5.7123	6.1932	6.3390	5.6599	5.6757	5.7020
Neves et al. [86]	5.4825	5.9600	6.1200	5.4950	5.5300	5.5625
Belabed et al. [104]	5.4800	5.9700	6.1200	5.5025	5.5350	5.5625
Alijani and Amabili [105]	5.4796	5.9578	6.1040	5.4919	5.5279	5.5633
Akavci and Tanrikulu [100]	5.4829	5.9676	6.1160	5.5064	5.5388	5.5644
Present	5.5172	6.0023	6.1505	5.5324	5.5642	5.5886

Table 8: Comparison of non-dimensional natural frequencies $\bar{\omega} = \omega \frac{a^2}{h}\sqrt{\frac{\rho}{E}}$ of SSSS homogeneous microplates

a/h	Theory	ℓ/h					
		0	0.2	0.4	0.6	0.8	1
5	CPT [36]	5.9734	6.4556	7.7239	9.4673	11.4713	13.6213
	TSDT [40]	5.2813	5.7699	7.0330	8.7389	10.6766	12.7408
	RPT (Present)	5.2813	5.7496	6.9667	8.6191	9.8943	9.9791
	Quasi-3D (Present)	5.3090	5.7622	6.9438	8.5509	9.8943	9.9791
20	CPT [36]	5.9734	6.4556	7.7239	9.4673	11.4713	13.6213
	TSDT [40]	5.9199	6.4027	7.6708	9.4116	11.4108	13.5545
	RPT (Present)	5.9199	6.4009	7.6646	9.4005	11.3945	13.5330
	Quasi-3D (Present)	5.9235	6.4030	7.6633	9.3952	11.3854	13.5202
100	CPT [36]	5.9734	6.4556	7.7239	9.4673	11.4713	13.6213
	TSDT [40]	5.9712	6.4535	7.7217	9.4651	11.4689	13.6186
	RPT (Present)	5.9712	6.4534	7.7215	9.4646	11.4682	13.6178
	Quasi-3D (Present)	5.9723	6.4544	7.7222	9.4650	11.4683	13.6177

Table 9: Non-dimensional natural frequency $\bar{\omega} = \omega \dfrac{a^2}{h}\sqrt{\dfrac{\rho_c}{E_c}}$ of SSSS Al/Al_2O_3 square plates (rule of mixtures scheme)

a/h	ℓ/h	$n=0$			$n=1$			$n=10$		
		RPT	Quasi-3D	TSDT[40]	RPT	Quasi-3D	TSDT[40]	RPT	Quasi-3D	TSDT[40]
5	0	5.2813	5.3090	5.2813	4.0781	4.1521	4.0781	3.2519	3.3126	3.2514
	0.2	5.7496	5.7622	5.7699	4.4959	4.5542	4.5094	3.5312	3.5740	3.5548
	0.4	6.9667	6.9438	7.0330	5.5620	5.5865	5.6071	4.2584	4.2627	4.3200
	0.6	8.6191	8.5509	8.7389	6.9822	6.9681	7.0662	5.2471	5.2115	5.3335
	0.8	9.8943	9.8943	10.6766	8.2313	8.2313	8.7058	5.8571	5.8571	6.4759
	1	9.9791	9.9791	12.7408	8.3019	8.3019	10.4397	5.9073	5.9073	7.6895
20	0	5.9199	5.9235	5.9199	4.5228	4.5919	4.5228	3.7623	3.8129	3.7622
	0.2	6.4009	6.4030	6.4027	4.9556	5.0179	4.9568	4.0299	4.0761	4.0323
	0.4	7.6646	7.6633	7.6708	6.0714	6.1203	6.0756	4.7428	4.7794	4.7488
	0.6	9.4005	9.3952	9.4116	7.5739	7.6107	7.5817	5.7369	5.7640	5.7453
	0.8	11.3945	11.3854	11.4108	9.2768	9.3042	9.2887	6.8914	6.9106	6.9013
	1	13.5330	13.5202	13.5545	11.0882	11.1082	11.1042	8.1384	8.1510	8.1494
100	0	5.9712	5.9723	5.9712	4.5579	4.6263	4.5579	3.8058	3.8533	3.8058
	0.2	6.4534	6.4544	6.4535	4.9922	5.0546	4.9922	4.0724	4.1168	4.0725
	0.4	7.7215	7.7222	7.7217	6.1124	6.1635	6.1126	4.7837	4.8215	4.7840
	0.6	9.4646	9.4650	9.4651	7.6220	7.6630	7.6224	5.7778	5.8090	5.7782
	0.8	11.4682	11.4683	11.4689	9.3339	9.3673	9.3344	6.9341	6.9600	6.9345
	1	13.6178	13.6177	13.6186	11.1554	11.1832	11.1560	8.1842	8.2060	8.1846

Table 10: The first six non-dimensional natural frequencies $\bar{\omega} = \omega \frac{a^2}{h}\sqrt{\frac{\rho_m}{E_m}}$ of Al/Al_2O_3 square plates (Mori-Tanaka scheme)

BC	a/h	Theory	Mode					
			1	2	3	4	5	6
SSSS	5	IGA-Zenkour	7.9366	13.8049	13.8049	17.3259	17.3259	19.5422
		Quasi-3D (Present)	7.8883	13.8049	13.8049	17.2045	17.2045	19.5422
		RPT (Present)	7.7844	13.8049	13.8049	16.9943	16.9943	19.5422
	10	IGA-Zenkour	8.5940	20.3230	20.3230	27.5893	27.5893	31.7475
		Quasi-3D (Present)	8.5607	20.2031	20.2031	27.5893	27.5893	31.5547
		RPT (Present)	8.4401	19.9188	19.9188	27.5893	27.5893	31.1386
	100	IGA-Zenkour	8.8399	21.7851	21.7851	35.3333	43.0764	43.0764
		Quasi-3D (Present)	8.8390	21.7802	21.7802	35.3221	43.0573	43.0573
		RPT (Present)	8.7127	21.4598	21.4598	34.8171	42.4074	42.4074
CCCC	5	IGA-Zenkour	12.7213	22.6661	22.6661	27.9021	27.9021	31.1450
		Quasi-3D (Present)	13.1029	22.9300	22.9300	27.8791	27.8791	31.3005
		RPT (Present)	12.1531	22.0683	22.0683	26.3182	26.3182	30.5398
	10	IGA-Zenkour	15.2379	28.9665	28.9665	41.2221	47.8649	47.9221
		Quasi-3D (Present)	15.4413	29.3267	29.3267	41.5955	48.2657	48.4504
		RPT (Present)	14.3638	27.8276	27.8276	39.9305	46.0435	46.4772
	100	IGA-Zenkour	16.0795	32.6473	32.6473	48.5912	58.0858	58.3951
		Quasi-3D (Present)	16.0540	32.6082	32.6082	48.5477	58.0353	58.3402
		RPT (Present)	15.5212	31.5708	31.5708	47.0903	56.2566	56.5207

Table 11: The first six non-dimensional natural frequencies $\bar{\omega} = \omega R^2\sqrt{\frac{\rho h}{D^\dagger}}$ of homogeneous circular microplates

ℓ/h	Theory	Mode					
		1	2	3	4	5	6
Simple support							
0	Mohammadi et al. [95]	4.9345	13.8981	25.6132	29.7198	39.9571	48.4788
	Nguyen et al. [91]	4.9304	13.8587	25.4798	29.5390	39.6331	48.0046
	RPT (Present)	4.9304	13.8591	25.4799	29.5456	39.6518	48.0402
	Quasi-3D (Present)	4.9385	13.8701	25.4983	29.5691	39.6881	48.0906
0.2	RPT (Present)	4.9925	14.5095	26.5426	31.1786	41.8855	50.8427
	Quasi-3D (Present)	5.0024	14.5206	26.5613	31.1981	41.9148	50.8808
0.4	RPT (Present)	5.1213	16.2743	29.4369	35.5996	47.7406	58.5547
	Quasi-3D (Present)	5.1365	16.2857	29.4529	35.6092	47.7542	58.5621
0.6	RPT (Present)	5.2422	18.8078	33.6370	41.9096	55.8684	69.6631
	Quasi-3D (Present)	5.2649	18.8192	33.6497	41.9065	55.8623	69.6331
0.8	RPT (Present)	5.3324	21.8342	38.6993	49.3881	65.3972	82.8177
	Quasi-3D (Present)	5.3642	21.8450	38.7080	49.3713	65.3694	82.7497
1	RPT (Present)	5.3954	25.1769	44.3292	57.5842	75.8223	97.1772
	Quasi-3D (Present)	5.4379	25.1869	44.3335	57.5538	75.7721	97.0720
Clamped support							
0	Mohammadi et al. [95]	10.2158	21.2604	34.8772	39.7706	51.0295	60.8290
	Nguyen et al. [91]	10.1839	21.1433	34.5892	39.3624	50.4385	59.9580
	RPT (Present)	10.1842	21.1459	34.5885	39.3832	50.4865	60.0416
	Quasi-3D (Present)	10.4466	21.6458	35.2774	40.2833	51.5045	61.3186
0.2	RPT (Present)	10.8087	22.4449	36.3961	41.8103	53.5802	63.7743
	Quasi-3D (Present)	11.0612	22.9236	37.1800	42.6664	54.5550	64.9738
0.4	RPT (Present)	12.4963	25.9527	41.2953	48.3406	61.7419	73.9729
	Quasi-3D (Present)	12.7255	26.3811	41.9956	49.0934	62.6149	74.9922
0.6	RPT (Present)	14.8897	30.9242	48.3696	57.5674	73.1139	88.5334
	Quasi-3D (Present)	15.0927	31.2968	48.9732	58.2073	73.8637	89.3634
0.8	RPT (Present)	17.7051	36.7699	56.8123	68.4011	86.4224	105.6689
	Quasi-3D (Present)	17.8850	37.0938	57.3265	68.9439	87.0506	106.3411
1	RPT (Present)	20.7715	43.1360	66.1009	80.1939	100.9243	124.3039
	Quasi-3D (Present)	20.9330	43.4206	66.5388	80.6591	101.4425	124.8498

$^\dagger D = \dfrac{Eh^3}{12(1-\nu^2)}$

Table 12: The first six non-dimensional natural frequencies $\bar{\omega} = \omega R^2 \sqrt{\frac{\rho_c h}{D_c^\dagger}}$ of Al/Al_2O_3 circular microplates (Mori-Tanaka scheme)

ℓ/h	Theory	Mode					
		1	2	3	4	5	6
Simple support							
0	IGA-Zenkour	3.4629	8.9254	8.9254	12.9890	12.9890	15.4780
	Quasi-3D (Present)	3.4132	8.8258	8.8258	12.9916	12.9916	15.3331
	RPT (Present)	3.3572	8.6722	8.6722	12.9121	12.9121	15.0490
0.2	IGA-Zenkour	3.5224	9.3961	9.3961	13.1894	13.1894	16.2612
	Quasi-3D (Present)	3.4675	9.2928	9.2928	13.1928	13.1928	16.1022
	RPT (Present)	3.4118	9.1595	9.1595	13.1037	13.1037	15.8706
0.4	IGA-Zenkour	3.6392	10.6411	10.6411	13.3115	13.3115	18.2644
	Quasi-3D (Present)	3.5698	10.5288	10.5288	13.3143	13.3143	18.1203
	RPT (Present)	3.5114	10.4415	10.4415	13.2326	13.2326	18.0361
0.6	IGA-Zenkour	3.7577	12.2959	12.2959	13.5601	13.5601	18.4956
	Quasi-3D (Present)	3.6687	12.1873	12.1873	13.5445	13.5445	18.4939
	RPT (Present)	3.6018	12.1378	12.1378	13.4872	13.4872	18.4475
0.8	IGA-Zenkour	3.8632	13.2220	13.2220	14.8766	14.8766	18.6662
	Quasi-3D (Present)	3.7546	13.2030	13.2030	14.7552	14.7552	18.6655
	RPT (Present)	3.6721	13.1245	13.1245	14.7850	14.7850	18.6192
1	IGA-Zenkour	3.9548	13.4288	13.4288	17.1268	17.1268	18.8623
	Quasi-3D (Present)	3.8303	13.4243	13.4243	16.9751	16.9751	18.8618
	RPT (Present)	3.9557	13.5531	13.5531	17.4735	17.4735	18.8633
Clamped support							
0	IGA-Zenkour	6.7718	12.9968	12.9968	19.8267	19.8608	21.9673
	Quasi-3D (Present)	6.8745	13.1770	13.1770	20.0202	20.0388	22.2840
	RPT (Present)	6.3384	12.4133	12.4133	19.0879	19.1363	20.9877
0.2	IGA-Zenkour	7.2163	13.9289	13.9289	21.1653	21.5889	23.7182
	Quasi-3D (Present)	7.3195	14.0950	14.0950	21.3095	21.7503	23.9885
	RPT (Present)	6.8208	13.4172	13.4172	20.5401	20.9799	22.8902
0.4	IGA-Zenkour	8.4091	16.4035	16.4035	24.6620	25.9011	25.9011
	Quasi-3D (Present)	8.5121	16.5390	16.5390	24.7273	25.8504	25.8504
	RPT (Present)	8.0909	16.0391	16.0391	24.2526	24.3345	24.3345
0.6	IGA-Zenkour	10.0860	19.8463	19.8463	25.9424	25.9424	28.6525
	Quasi-3D (Present)	10.1880	19.9431	19.9431	25.8948	25.8948	28.6525
	RPT (Present)	9.8463	19.6321	19.6321	24.3655	24.3655	28.6525
0.8	IGA-Zenkour	12.0447	23.8379	23.8379	25.9920	25.9920	28.9380
	Quasi-3D (Present)	12.1441	23.8850	23.8850	25.9507	25.9507	28.9380
	RPT (Present)	11.8741	23.7016	23.7016	24.4627	24.4627	28.9380
1	IGA-Zenkour	14.1674	26.0476	26.0476	28.1435	28.1435	29.3010
	Quasi-3D (Present)	14.2615	25.9953	25.9953	28.1492	28.1492	29.3010
	RPT (Present)	14.0568	24.4150	24.4150	28.2217	28.2217	29.3010

$^\dagger D_c = \dfrac{E_c h^3}{12(1-\nu_c^2)}$

Table 13: Comparison of non-dimensional critical buckling loads $\bar{P}_{cr} = \dfrac{P_{cr}a^2}{E_2h^3}$ of square FG microplates (rule of mixtures scheme)

ℓ/h	Theory	$a/h=5$			$a/h=10$			$a/h=20$		
		$n=0$	$n=1$	$n=10$	$n=0$	$n=1$	$n=10$	$n=0$	$n=1$	$n=10$
0	CPT [41]	19.2255	8.2145	3.8359	19.2255	8.2145	3.8359	19.2255	8.2145	3.8359
	FSDT [41]	15.3228	6.8576	2.9979	18.0746	7.8273	3.5853	18.9243	8.1142	3.7700
	RPT [45]	15.3322	6.8611	2.7672	18.0754	7.8276	3.4969	18.9243	8.1142	3.7450
	RPT (Present)	15.3321	6.8610	2.7702	18.0756	7.8277	3.4982	18.9244	8.1143	3.7454
	Quasi-3D (Present)	15.3629	7.3905	3.0118	18.1561	8.5396	3.8921	18.9675	8.8639	4.1850
0.2	CPT [41]	22.0863	9.7879	4.3560	22.0863	9.7879	4.3560	22.0863	9.7879	4.3560
	FSDT [41]	17.6150	8.1715	3.4076	20.7607	9.3241	4.0710	21.7387	9.6675	4.2809
	RPT [45]	18.0422	8.3399	3.3619	20.9025	9.3767	4.0513	21.7771	9.6815	4.2752
	RPT (Present)	17.8878	8.2820	3.2917	20.8497	9.3581	4.0246	21.7628	9.6766	4.2677
	Quasi-3D (Present)	17.7286	8.7153	3.4728	20.8583	10.0344	4.3958	21.7852	10.4160	4.7009
0.4	CPT [41]	30.6685	14.5082	5.9164	30.6685	14.5082	5.9164	30.6685	14.5082	5.9164
	FSDT [41]	24.2899	11.9922	4.6013	28.7478	13.7742	5.5151	30.1625	14.3167	5.8102
	RPT [45]	26.1539	12.7754	5.0407	29.3735	14.0232	5.6631	30.3324	14.3832	5.8505
	RPT (Present)	25.5457	12.5322	4.8371	29.1700	13.9459	5.5925	30.2773	14.3626	5.8312
	Quasi-3D (Present)	24.8060	12.6741	4.8557	28.9624	14.5168	5.9066	30.2381	15.0722	6.2486
0.6	CPT [41]	44.9723	22.3753	8.5171	44.9723	22.3753	8.5171	44.9723	22.3753	8.5171
	FSDT [41]	34.7856	17.9838	6.4804	41.8271	21.0597	7.8802	44.1369	22.0292	8.3472
	RPT [45]	39.6393	20.1658	7.7001	43.4732	21.7657	8.2906	44.5855	22.2188	8.4589
	RPT (Present)	38.2867	19.5858	7.3772	43.0329	21.5846	8.1871	44.4673	22.1708	8.4312
	Quasi-3D (Present)	36.5415	19.2256	7.1597	42.4620	21.9814	8.4246	44.3258	22.8320	8.8281
0.8	CPT [41]	64.9976	33.3892	12.1581	64.9976	33.3892	12.1581	64.9976	33.3892	12.1581
	FSDT [41]	48.2915	25.6654	8.9020	59.6657	30.9928	11.1065	63.5656	32.7517	11.8745
	RPT [45]	58.4862	30.5105	11.3322	63.1958	32.6036	11.9349	64.5348	33.1882	12.1011
	RPT (Present)	56.0961	29.4240	10.9005	62.4358	32.2693	11.8036	64.3321	33.0999	12.0666
	Quasi-3D (Present)	52.8623	28.3151	10.3843	61.3467	32.4199	11.9498	64.0474	33.6948	12.4394
1	CPT [41]	90.7444	47.5499	16.8393	90.7444	47.5499	16.8393	-	-	-
	FSDT [41]	63.8913	34.4981	11.7042	81.8269	43.3274	15.1152	-	-	-
	RPT [45]	82.6938	43.8094	15.9522	88.5416	46.5372	16.6033	90.1804	47.2914	16.7793
	RPT (Present)	78.9675	42.0388	15.4071	87.3775	45.9981	16.4431	89.8715	47.1494	16.7376
	Quasi-3D (Present)	73.6925	39.8872	14.5287	85.6043	45.8223	16.4819	89.4018	47.6596	17.0825

Table 14: Non-dimensional critical buckling load $\bar{P}_{cr} = \dfrac{P_{cr}a^2}{D_m^{\dagger}}$ of Al/Al_2O_3 square microplates (Mori-Tanaka scheme)

BC	a/h	ℓ/h	$n=0$		$n=1$		$n=10$	
			RPT	Quasi-3D	RPT	Quasi-3D	RPT	Quasi-3D
SSSS	5	0	87.4747	86.5475	35.0795	35.6610	21.7236	21.7189
		0.2	103.6359	101.8797	42.3816	42.6185	25.4909	25.2307
		0.4	152.0215	147.6312	64.2668	63.3902	36.7873	35.7417
		0.6	232.4351	223.1633	100.6957	97.7189	55.6034	53.1891
		0.8	344.7280	327.6683	151.6424	145.2904	81.9336	77.4961
		1	488.8378	460.3907	217.0988	205.8260	115.7764	108.5941
	20	0	105.6668	105.6221	42.0033	43.4065	27.5182	27.8578
		0.2	123.5339	123.4102	49.9504	51.3272	31.5521	31.8705
		0.4	177.1295	176.7715	73.7907	75.0881	43.6520	43.9085
		0.6	266.4425	265.6972	113.5226	114.6856	63.8152	63.9707
		0.8	391.4648	390.1733	169.1451	170.1141	92.0401	92.0558
		1	552.1931	550.1813	240.6580	241.3659	128.3267	128.1618
	100	0	107.0958	107.1271	42.5423	44.0165	27.9978	28.3566
		0.2	125.0926	125.1206	50.5370	52.0102	32.0486	32.4065
		0.4	179.0825	179.1009	74.5212	75.9913	44.2009	44.5563
		0.6	269.0653	269.0682	114.4947	115.9596	64.4546	64.8061
		0.8	395.0406	395.0223	170.4576	171.9154	92.8097	93.1557
		1	557.0082	556.9633	242.4098	243.8584	129.2661	129.6052
CCCC	5	0	178.2578	188.3478	72.2150	78.0421	42.1220	45.4860
		0.2	206.9297	215.7331	85.4028	90.6731	49.1101	52.1032
		0.4	292.6287	295.5433	124.8630	127.4320	69.9984	71.1001
		0.6	435.0030	424.8837	190.5274	187.0650	104.7011	101.8084
		0.8	633.8611	601.6084	282.3839	268.7548	153.1709	144.0664
		1	889.1171	823.8983	400.4310	371.8457	215.3906	197.7752
	20	0	273.9507	288.6976	109.0237	117.3906	70.8926	75.2177
		0.2	308.7803	323.9291	124.5481	133.0578	78.8262	83.2085
		0.4	413.0833	429.0109	171.0330	179.8054	102.5575	107.0378
		0.6	586.6304	603.0356	248.3764	257.2793	141.9833	146.4815
		0.8	829.3607	845.5938	356.5558	365.3387	197.0586	201.4295
		1	1141.2885	1156.5929	495.5793	503.9582	267.7793	271.8584
	100	0	283.7646	292.2008	112.7294	119.3117	74.1644	77.0743
		0.2	319.1326	327.9091	128.4414	135.1344	82.1289	85.1055
		0.4	425.0550	434.6081	175.4917	182.4322	105.9838	109.1182
		0.6	601.2918	611.6685	253.7742	260.9696	145.6726	148.9836
		0.8	847.7694	858.8291	363.2623	370.6627	201.1735	204.6383
		1	1164.4998	1176.0787	503.9643	511.5167	272.4865	276.0730

$^{\dagger}D_m = \dfrac{E_m h^3}{12(1-\nu_m^2)}$

Table 15: The first six non-dimensional buckling loads $\bar{P} = \dfrac{Pa^2}{D_m}$ of Al/Al_2O_3 square microplates, $n = 10$, $\ell/h = 0.2$ (Mori-Tanaka scheme)

BC	a/h	Theory	Mode					
			1	2	3	4	5	6
SSSS	5	IGA-Zenkour	25.4064	47.0158	47.0158	62.7947	66.4706	66.4706
		Quasi-3D (Present)	25.2307	46.2828	46.2828	61.4689	64.8256	64.8256
		RPT (Present)	25.4909	47.9306	47.9306	64.7895	68.7456	68.7456
	10	IGA-Zenkour	30.3554	67.5835	67.5835	101.6321	115.5866	115.5866
		Quasi-3D (Present)	30.2890	67.2254	67.2254	100.9300	114.4706	114.4706
		RPT (Present)	30.1012	67.3570	67.3570	101.9693	116.1512	116.1512
	20	IGA-Zenkour	31.8815	76.0319	76.0319	121.4313	143.5095	143.5095
		Quasi-3D (Present)	31.8705	75.8988	75.8988	121.1662	143.0021	143.0021
		RPT (Present)	31.5521	75.2628	75.2628	120.4131	142.2468	142.2468
	100	IGA-Zenkour	32.3844	79.0722	79.0722	129.2976	155.1773	155.1773
		Quasi-3D (Present)	32.4065	79.1198	79.1198	129.3662	155.2457	155.2457
		RPT (Present)	32.0486	78.2296	78.2296	127.9519	153.4678	153.4678
CCCC	5	IGA-Zenkour	50.6557	66.0350	66.0350	78.0114	80.2597	84.0819
		Quasi-3D (Present)	52.1032	66.3156	66.3156	77.2179	78.9774	84.1043
		RPT (Present)	49.1101	66.7907	66.7907	80.3088	82.9464	85.5400
	10	IGA-Zenkour	74.8665	114.2196	114.2196	146.4170	160.1781	172.6816
		Quasi-3D (Present)	75.4661	115.7598	115.7598	147.8696	161.3725	174.2442
		RPT (Present)	70.1001	110.6293	110.6293	144.4919	158.8413	167.4729
	20	IGA-Zenkour	83.8952	140.5084	140.5084	191.9601	219.4306	239.0973
		Quasi-3D (Present)	83.2085	140.4610	140.4610	192.6237	220.3776	239.1104
		RPT (Present)	78.8262	133.9531	133.9531	185.0964	211.8925	227.4324
	100	IGA-Zenkour	85.2475	149.0723	149.0723	210.8794	246.4373	267.8293
		Quasi-3D (Present)	85.1055	148.8861	148.8861	210.7133	246.2408	267.4391
		RPT (Present)	82.1289	143.8128	143.8128	203.9109	237.9639	257.7571

Table 16: Comparison of non-dimensional critical buckling loads $\bar{P_{cr}} = \dfrac{P_{cr}R^2}{D_m}$ of CCCC Al/ZrO_2-2 circular plates (rule of mixtures scheme)

n	Theory	h/R			
		0.1	0.2	0.25	0.3
0	TSDT [96]	14.089	12.574	11.638	10.670
	UTSDT [97]	14.089	12.575	11.639	10.670
	TSDT [98]	14.1089	12.5914	11.6540	10.6842
	RPT [63]	14.2023	12.7281	11.8143	10.8666
	RPT (Present)	14.0932	12.5776	11.6409	10.6719
	Quasi-3D (Present)	14.8264	13.4557	12.4564	11.3775
0.5	TSDT [96]	19.411	17.311	16.013	14.672
	UTSDT [97]	19.413	17.310	16.012	14.672
	TSDT [98]	19.4391	17.3327	16.0334	14.6910
	RPT [63]	19.5663	17.5180	16.2506	14.9381
	RPT (Present)	19.4169	17.3133	16.0153	14.6740
	Quasi-3D (Present)	20.5166	18.6074	17.2206	15.7222
2	TSDT [96]	23.074	20.803	19.377	17.882
	UTSDT [97]	23.075	20.805	19.378	17.881
	TSDT [98]	23.1062	20.8319	19.4033	17.9060
	RPT [63]	23.2592	21.0569	19.6687	18.2099
	RPT (Present)	23.0809	20.8088	19.3812	17.8848
	Quasi-3D (Present)	24.4332	22.3510	20.8035	19.1161
5	TSDT [96]	25.439	22.971	21.414	19.780
	UTSDT [97]	25.442	22.969	21.412	19.778
	TSDT [98]	25.4743	22.9992	21.4407	19.8043
	RPT [63]	25.6418	23.2426	21.7268	20.1313
	RPT (Present)	25.4469	22.9742	21.4168	19.7813
	Quasi-3D (Present)	26.8812	24.6195	22.9303	21.0878
10	TSDT [96]	27.133	24.423	22.725	20.948
	UTSDT [97]	27.131	24.422	22.725	20.949
	TSDT [98]	27.1684	24.4542	22.7536	20.9750
	RPT [63]	27.3429	24.6994	23.0389	21.2986
	RPT (Present)	27.1395	24.4287	22.7297	20.9524
	Quasi-3D (Present)	28.6197	26.1483	24.3140	22.3196

Table 17: Non-dimensional critical buckling loads $\bar{P_{cr}} = \dfrac{P_{cr}R^2}{D_m}$ of Al/Al_2O_3 circular microplates (Mori-Tanaka scheme)

h/R	ℓ/h	$n=0$		$n=1$		$n=10$	
		RPT	Quasi-3D	RPT	Quasi-3D	RPT	Quasi-3D
Simple support							
0.1	0	22.5182	22.6953	9.5368	9.7960	5.9574	6.0309
	0.2	23.0489	23.2627	9.8179	10.0793	6.0876	6.1617
	0.4	24.1022	24.4172	10.3474	10.6292	6.3543	6.4360
	0.6	25.0682	25.5337	10.8125	11.1391	6.6130	6.7163
	0.8	25.7985	26.4629	11.1543	11.5512	6.8182	6.9619
	1	26.3291	27.2420	11.3981	11.8897	6.9718	7.1752
0.2	0	21.7456	22.0263	9.2059	9.4510	5.6942	5.7510
	0.2	22.2719	22.5928	9.4873	9.7327	5.8318	5.8833
	0.4	23.2739	23.7059	9.9893	10.2520	6.1019	6.1509
	0.6	24.2066	24.8190	10.4423	10.7545	6.3676	6.4377
	0.8	24.9581	25.8386	10.8003	11.2074	6.5891	6.7170
	1	25.5480	26.7897	11.0777	11.6254	6.7647	6.9866
0.3	0	20.5707	20.8606	8.7033	8.9036	5.3041	5.3287
	0.2	21.0993	21.4128	8.9860	9.1777	5.4526	5.4621
	0.4	22.0854	22.4669	9.4810	9.6686	5.7409	5.7276
	0.6	23.0439	23.5641	9.9511	10.1693	6.0352	6.0281
	0.8	23.8746	24.6485	10.3517	10.6610	6.2927	6.3431
	1	24.5707	25.7228	10.6823	11.1443	6.5055	6.6623
Clamped support							
0.1	0	76.5059	80.4859	30.4539	32.7398	19.7743	20.9413
	0.2	86.3696	90.4095	34.8524	37.1578	22.0235	23.1967
	0.4	115.9595	120.0466	48.0474	50.3612	28.7616	29.9236
	0.6	165.2737	169.2564	70.0379	72.3004	39.9728	41.0821
	0.8	234.3115	237.9906	100.8235	102.9597	55.6486	56.6598
	1	323.0727	326.2293	140.4042	142.3316	75.7879	76.6551
0.2	0	68.2782	73.0452	27.3245	29.8617	17.1442	18.6240
	0.2	77.6521	82.3859	31.5460	34.0702	19.3412	20.7979
	0.4	105.7687	110.0650	44.2098	46.5462	25.9122	27.1925
	0.6	152.6199	155.7501	65.3154	67.1544	36.8218	37.7110
	0.8	218.1997	219.2330	94.8629	95.8167	52.0495	52.3297
	1	302.5060	300.3159	132.8523	132.4584	71.5905	71.0373
0.3	0	57.9331	61.7636	23.3438	25.4648	14.0464	15.3047
	0.2	66.6302	70.2136	27.3083	29.3268	16.1359	17.3213
	0.4	92.7032	95.0207	39.2004	40.6571	22.3875	23.1508
	0.6	136.1160	135.6444	59.0182	59.2280	32.7704	32.6634
	0.8	196.8399	191.6493	86.7603	84.8742	47.2643	45.8312
	1	274.8619	262.6208	122.4264	117.4429	65.8628	62.6312

Table 18: The first six non-dimensional buckling loads $\bar{P} = \dfrac{PR^2}{D_m}$ of Al/Al_2O_3 circular microplates, $n = 1$, $\ell/h = 0.6$ (Mori-Tanaka scheme)

BC	h/R	Theory	Mode					
			1	2	3	4	5	6
Simple support	0.1	IGA-Zenkour	11.4689	54.8031	54.8031	95.3143	123.2488	129.6396
		Quasi-3D (Present)	11.1391	54.0884	54.0884	93.7842	122.0854	128.1298
		RPT (Present)	10.8125	53.6215	53.6215	93.3944	122.3489	128.3281
	0.2	IGA-Zenkour	11.3113	50.7663	50.7663	83.1176	107.1987	110.9343
		Quasi-3D (Present)	10.7545	49.5358	49.5358	80.6606	104.8026	108.1436
		RPT (Present)	10.4423	50.2378	50.2378	83.3889	109.1766	112.9355
	0.3	IGA-Zenkour	10.8014	45.2015	45.2015	69.1649	89.4125	90.9795
		Quasi-3D (Present)	10.1693	43.6917	43.6917	66.3080	86.1911	87.4685
		RPT (Present)	9.9511	45.6739	45.6739	71.5215	93.8041	95.5819
Clamped support	0.1	IGA-Zenkour	72.6509	126.0657	126.0657	172.3464	205.4419	222.4846
		Quasi-3D (Present)	72.3004	125.7477	125.7477	171.5372	205.0589	221.0537
		RPT (Present)	70.0379	123.1185	123.1185	169.2944	203.3425	218.6139
	0.2	IGA-Zenkour	66.8949	108.9270	108.9270	140.4481	166.8569	175.2599
		Quasi-3D (Present)	67.1544	108.3685	108.3685	138.0488	164.4947	172.3137
		RPT (Present)	65.3154	109.4813	109.4813	143.4150	171.7706	179.5962
	0.3	IGA-Zenkour	58.9576	90.1444	90.1444	110.5155	131.5270	134.2574
		Quasi-3D (Present)	59.2280	88.4285	88.4285	106.6289	127.0395	129.6436
		RPT (Present)	59.0182	93.6789	93.6789	117.0824	140.3857	143.1361

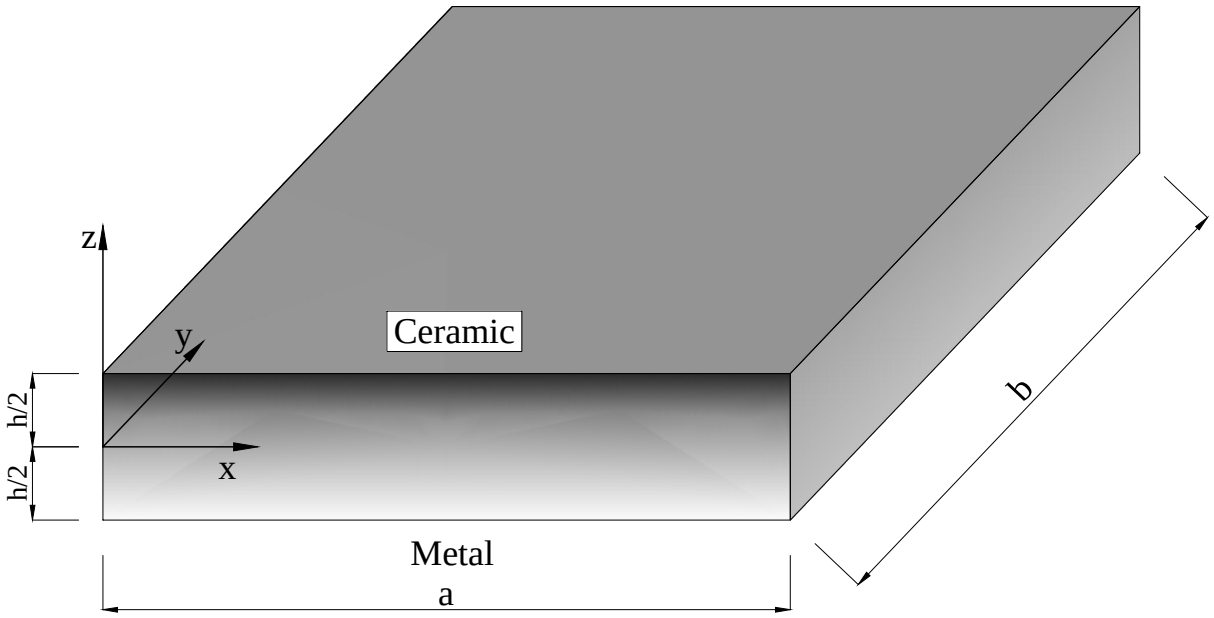

Figure 1: The functionally graded microplate model.

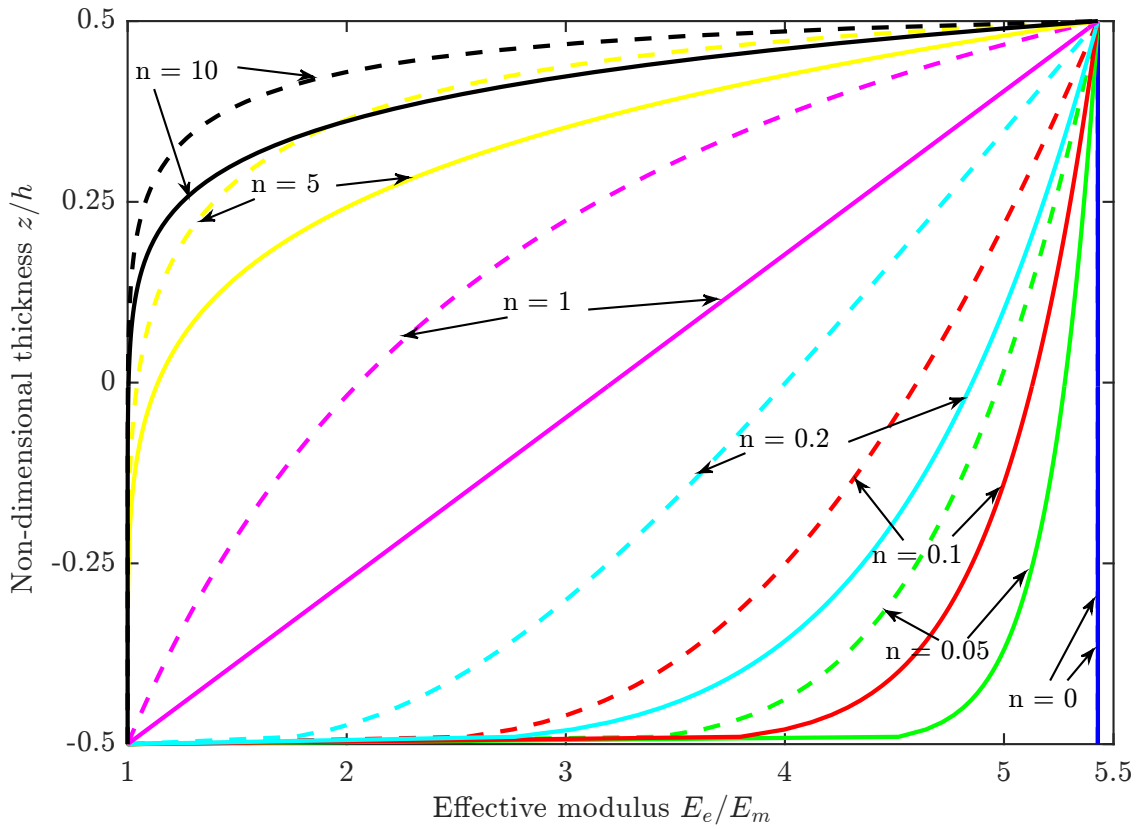

Figure 2: The effective modulus of Al/Al_2O_3 plates according to the rule of mixtures scheme (in solid lines) and Mori-Tanaka scheme (in dash lines).

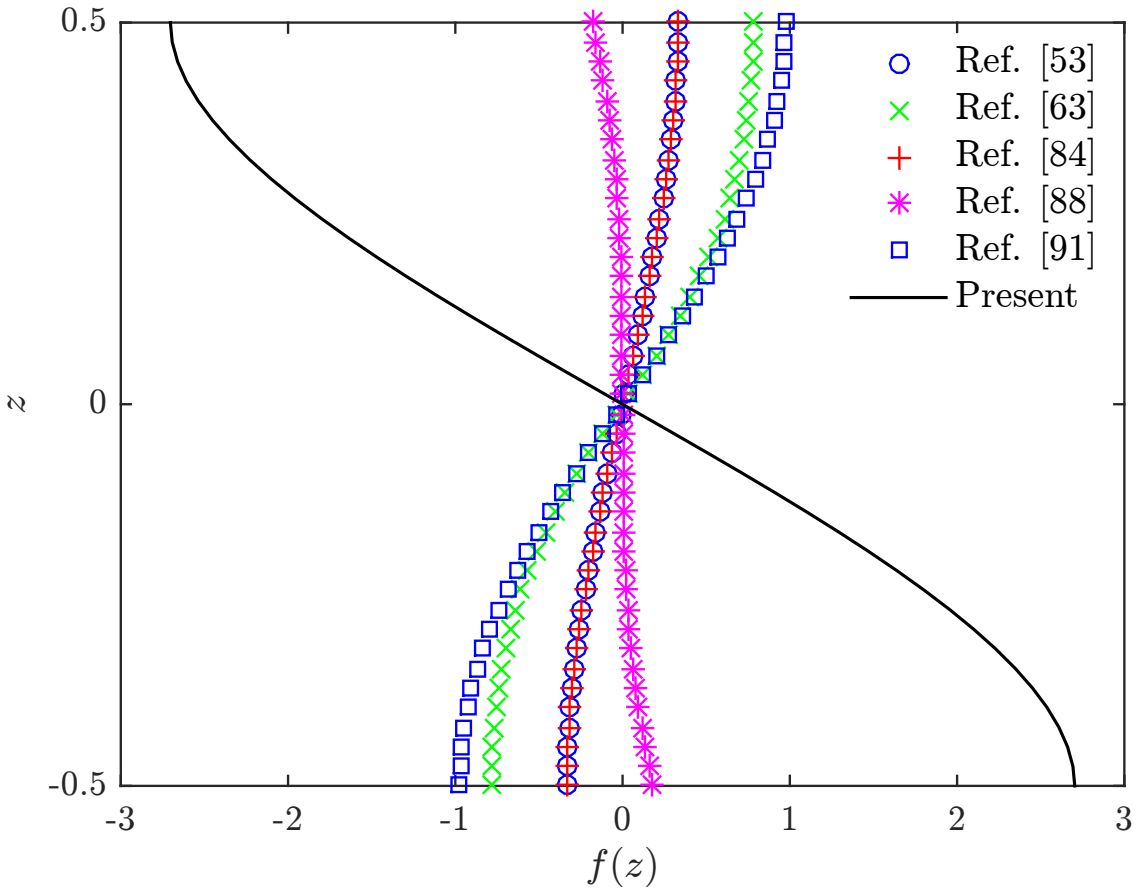

Figure 3: Distribution function f.

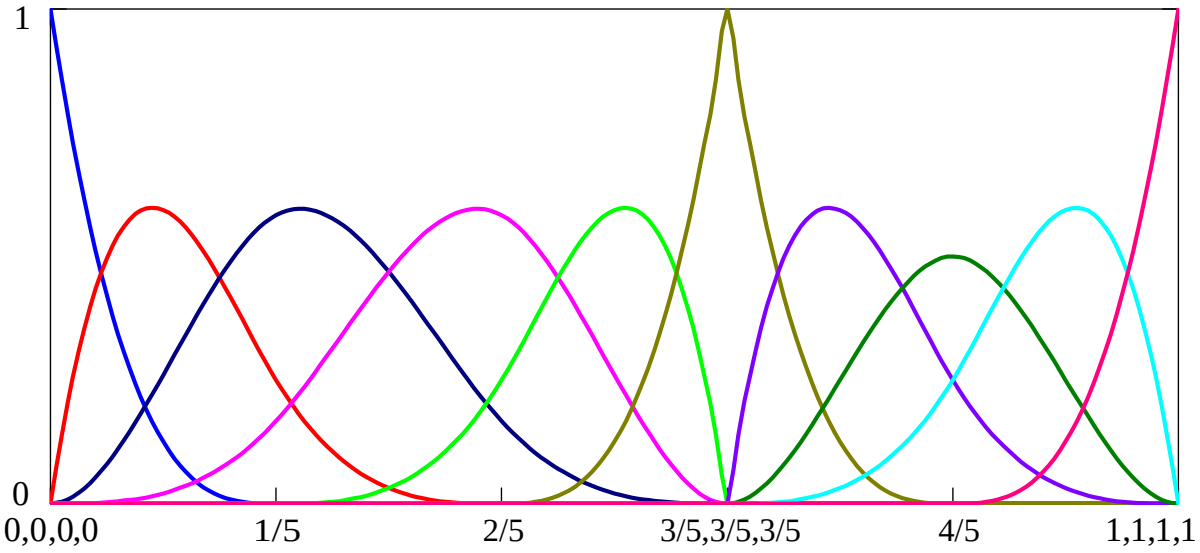

(a) Cubic basis functions corresponding to $\boldsymbol{\Xi} = \{0, 0, 0, 0, \frac{1}{5}, \frac{2}{5}, \frac{3}{5}, \frac{3}{5}, \frac{3}{5}, \frac{4}{5}, 1, 1, 1, 1\}$.

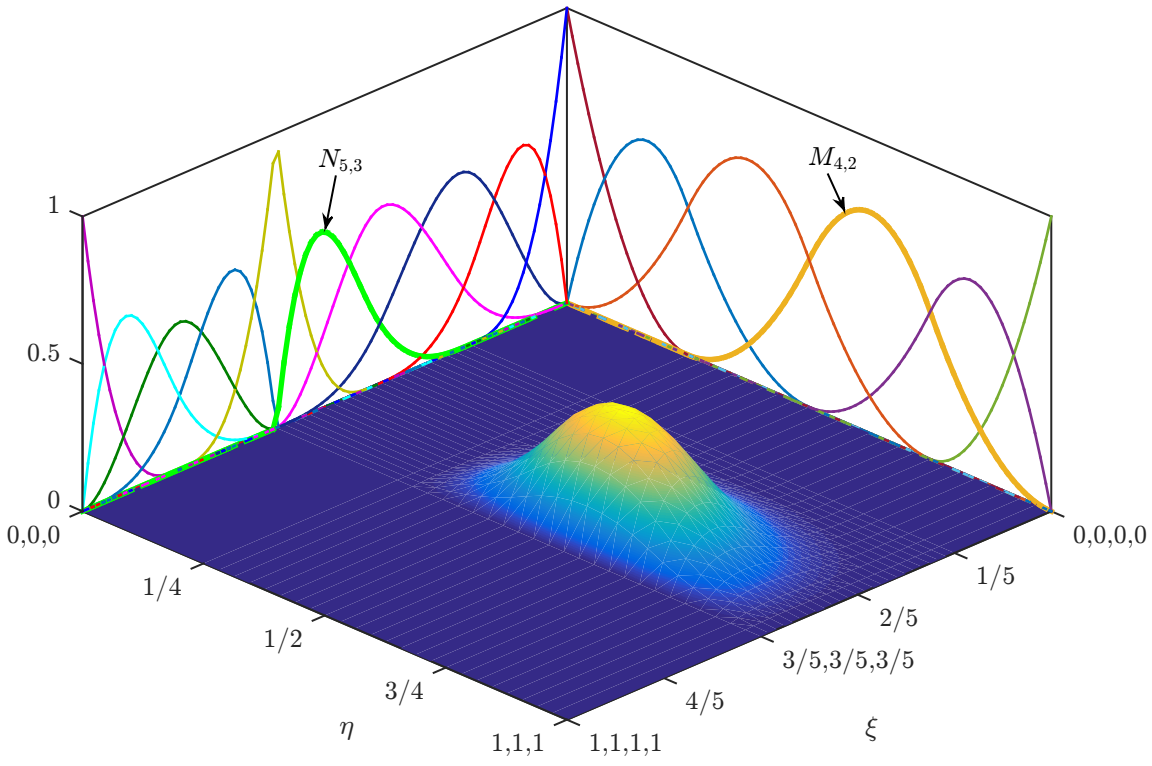

(b) Bivariate B-spline basis functions.

Figure 4: One- and two-dimensional B-spline basis functions.

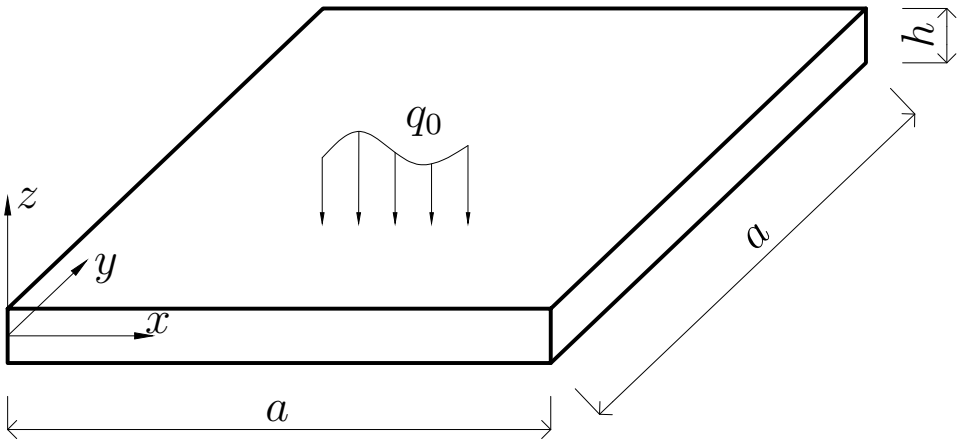

(a) Geometric configuration.

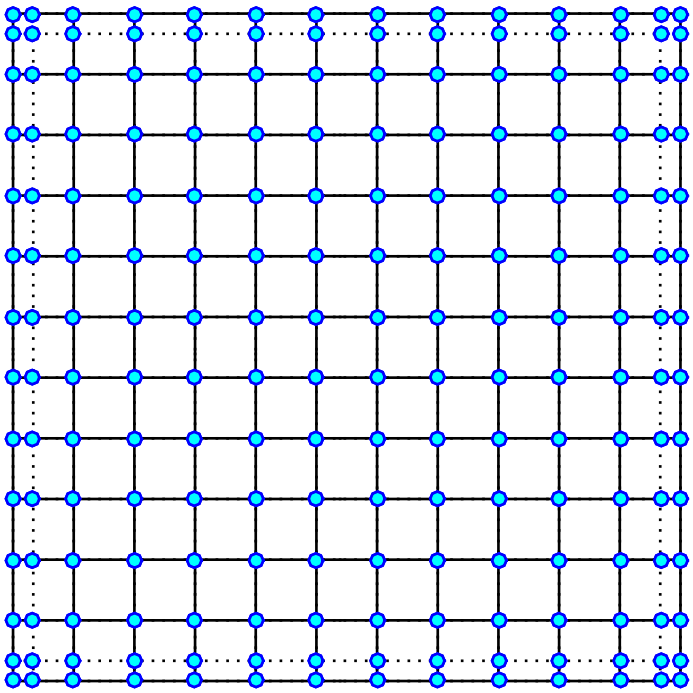

(b) Control point net and 11×11 cubic elements.

Figure 5: Geometry and element mesh of a square microplate.

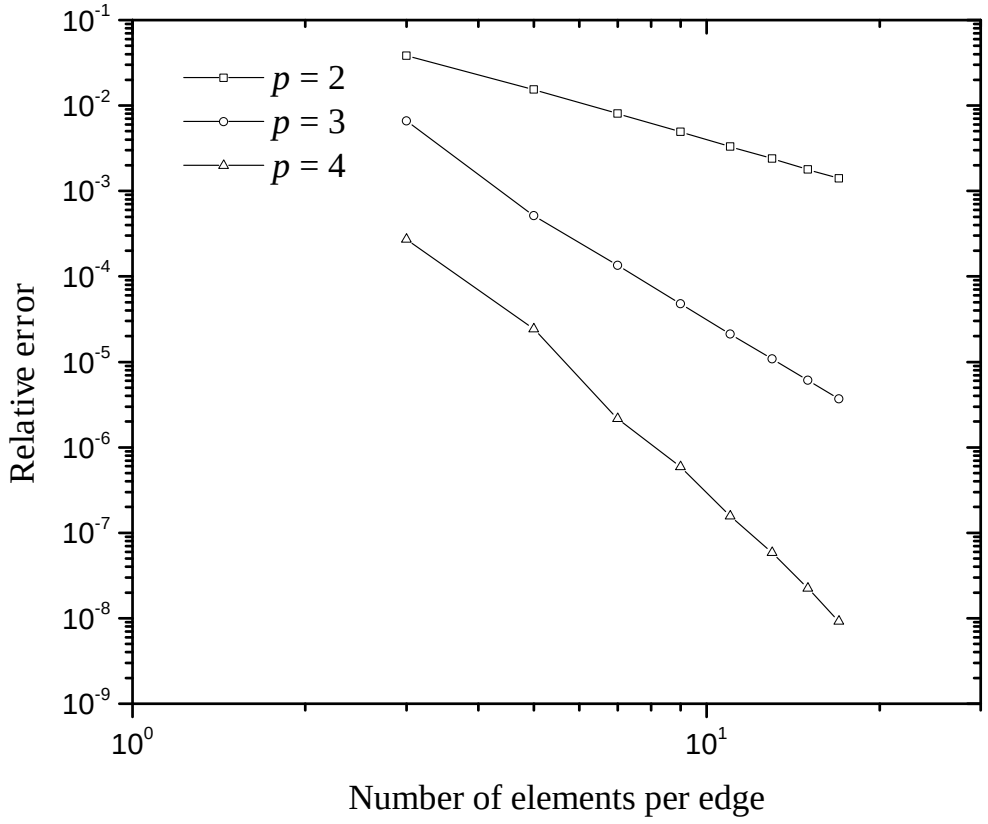

Figure 6: Relative error of non-dimensional central deflection of homogeneous square microplates.

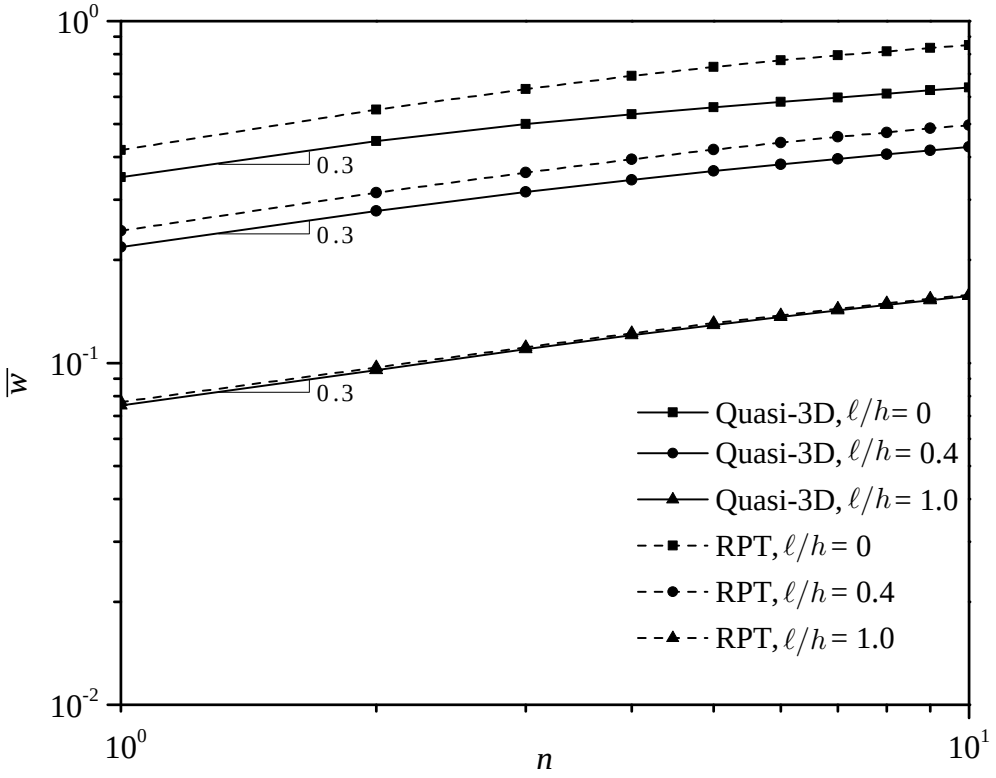

Figure 7: Effects of material index n and material length scale ratio ℓ/h on the central deflection of CCCC Al/Al_2O_3 square microplates subjected to uniformly distributed load, $a/h = 5$ (rule of mixtures scheme).

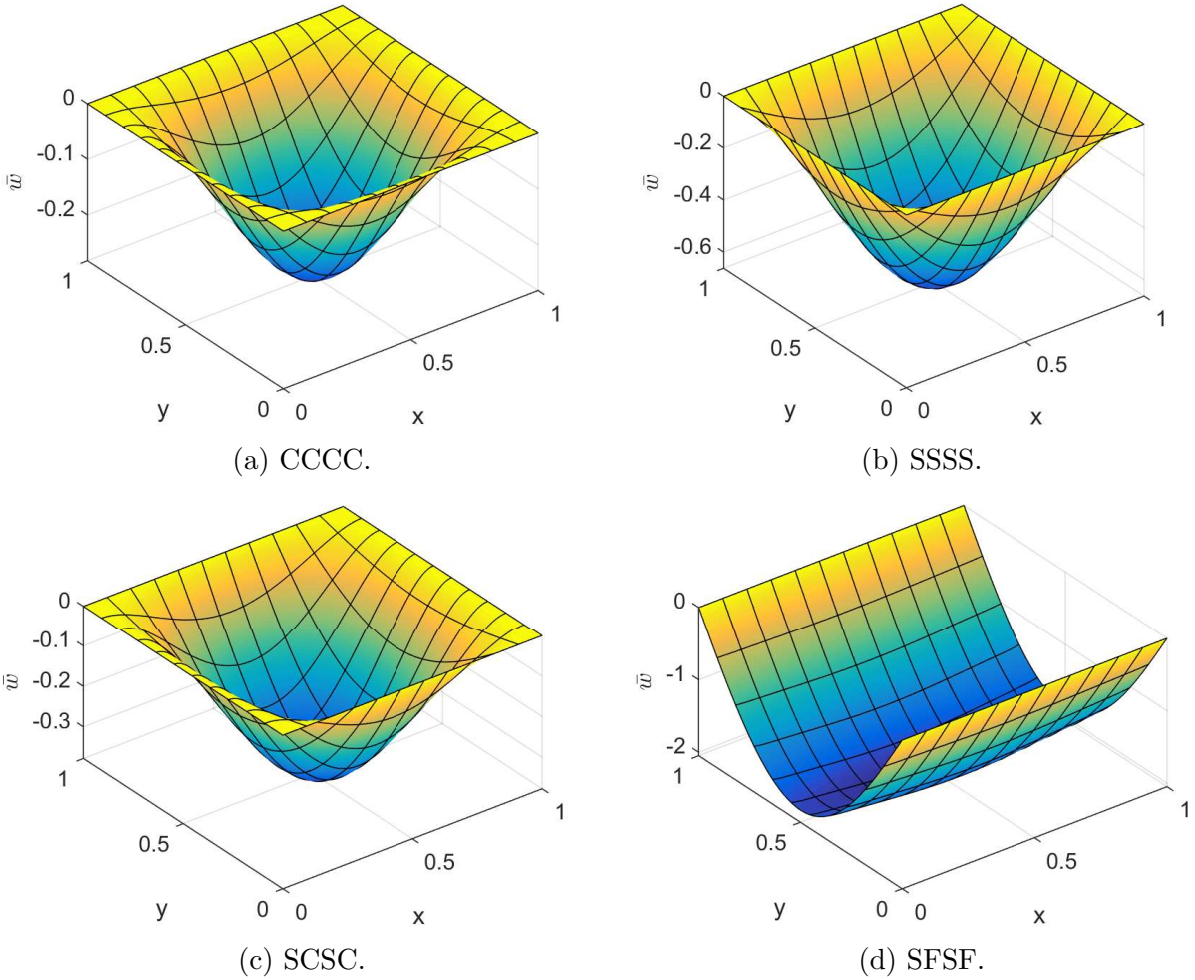

(a) CCCC. (b) SSSS.

(c) SCSC. (d) SFSF.

Figure 8: Deformed configuration of Al/Al_2O_3 square microplates.

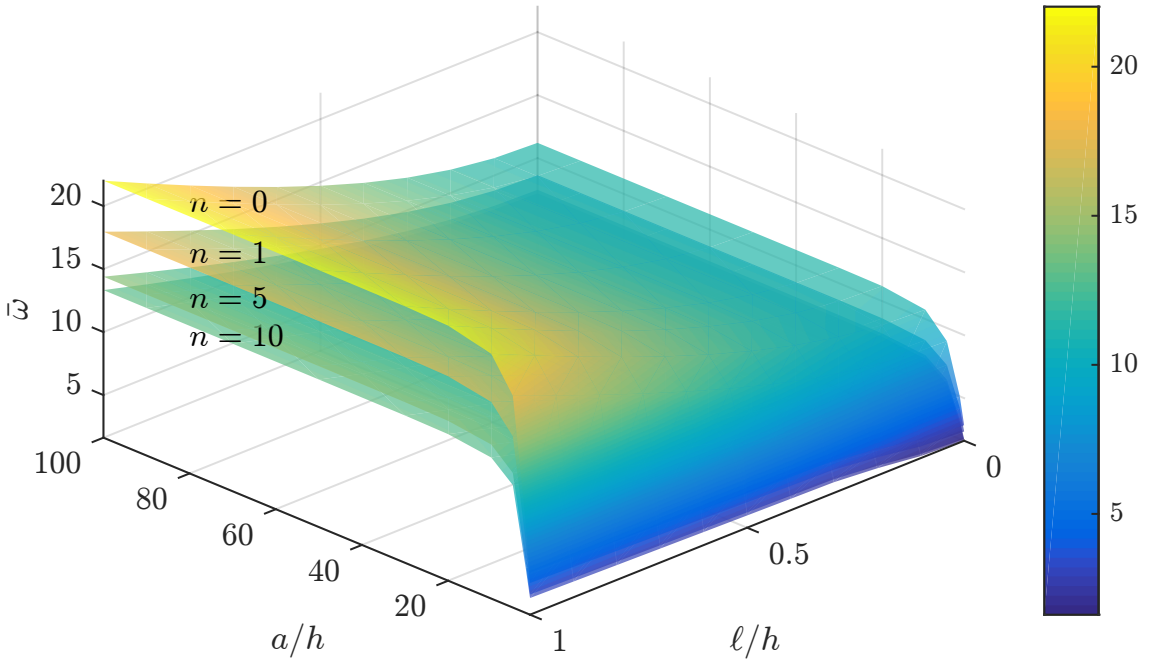

Figure 9: Variation of natural frequency of CCCC Al/Al_2O_3 square microplates (rule of mixtures scheme).

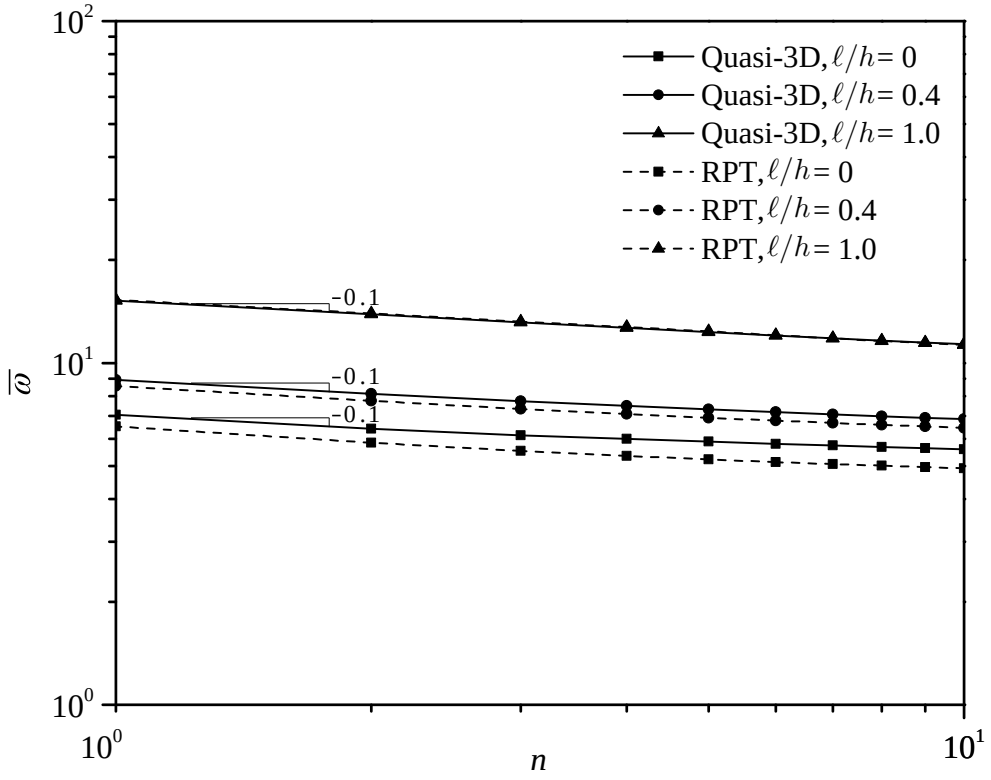

Figure 10: Effects of material index n and material length scale ratio ℓ/h on the natural frequency of CCCC Al/Al_2O_3 square microplates, $a/h = 5$ (rule of mixtures scheme).

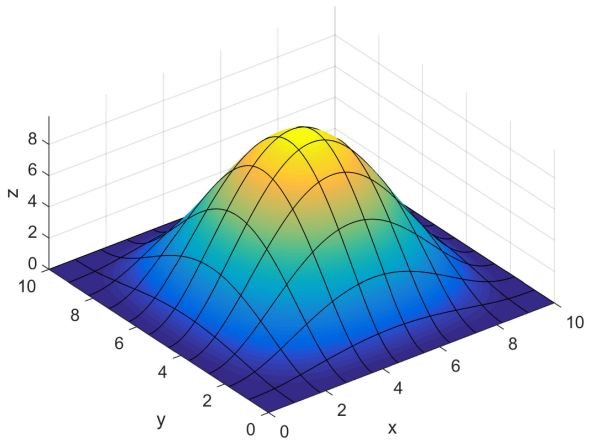

(a) $\bar{\omega}_1 = 15.4413$.

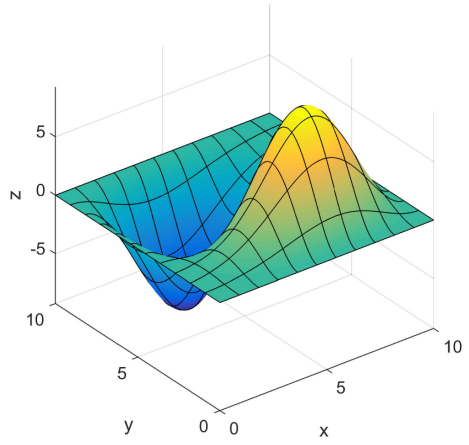

(b) $\bar{\omega}_2 = 29.3267$.

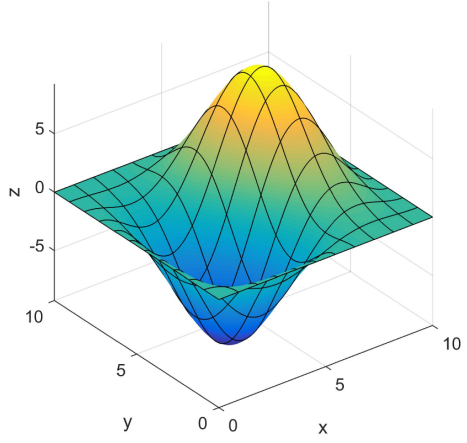

(c) $\bar{\omega}_3 = 29.3267$.

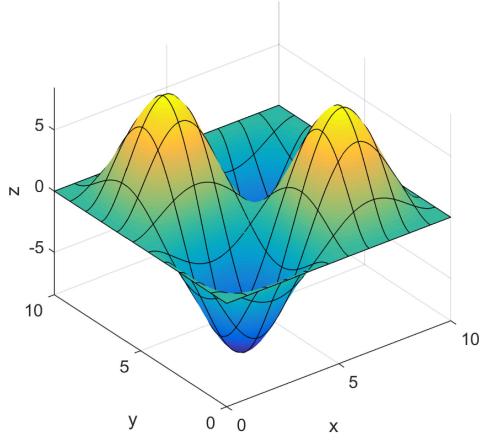

(d) $\bar{\omega}_4 = 41.5955$.

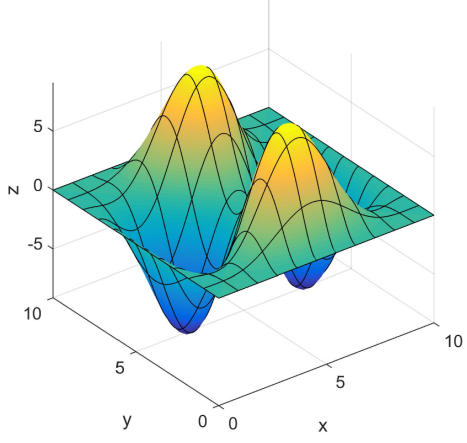

(e) $\bar{\omega}_5 = 48.2657$.

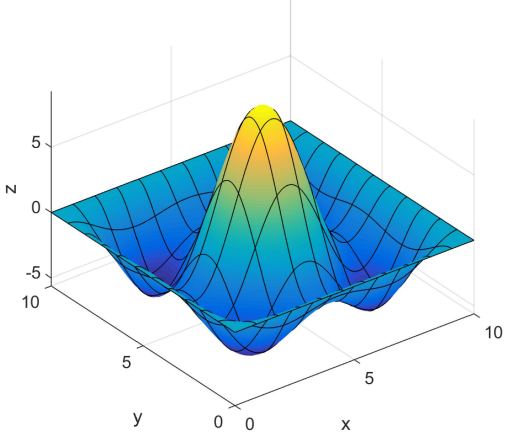

(f) $\bar{\omega}_6 = 48.4504$.

Figure 11: The first six free vibration mode shapes of Al/Al_2O_3 CCCC square microplates.

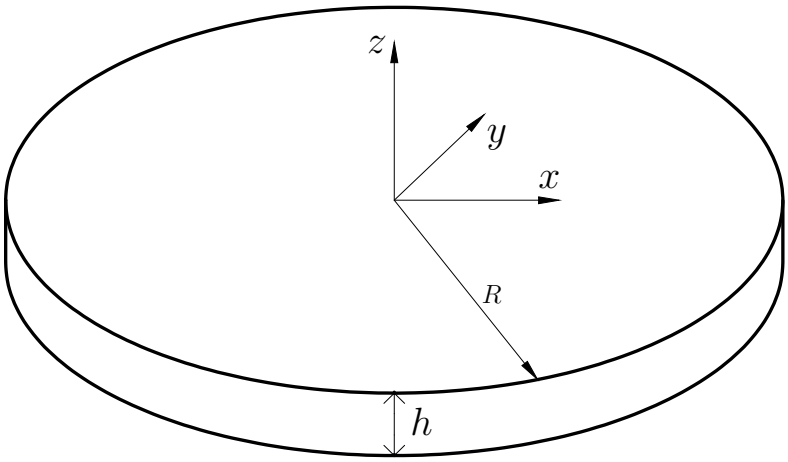

(a) Geometric configuration.

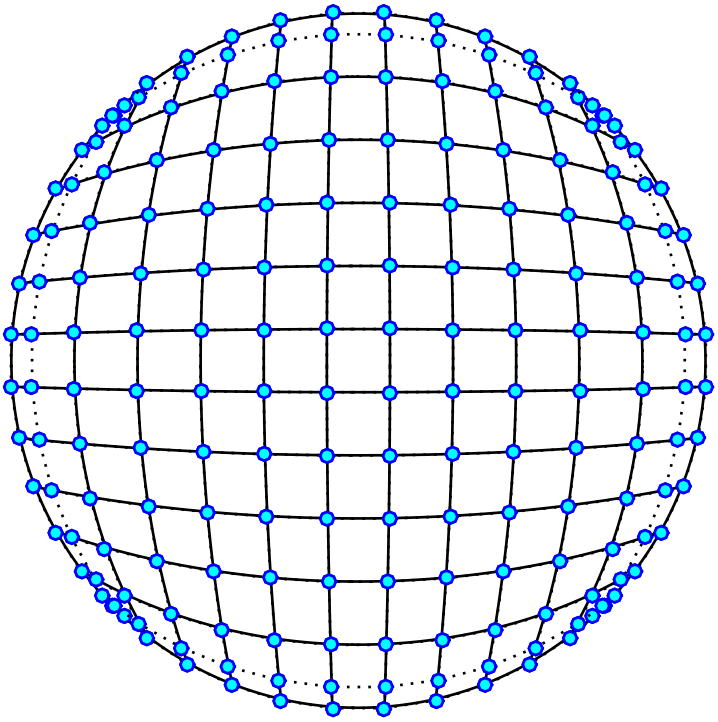

(b) Control point net and 11×11 cubic elements.

Figure 12: Geometry and element mesh of a circular microplate.

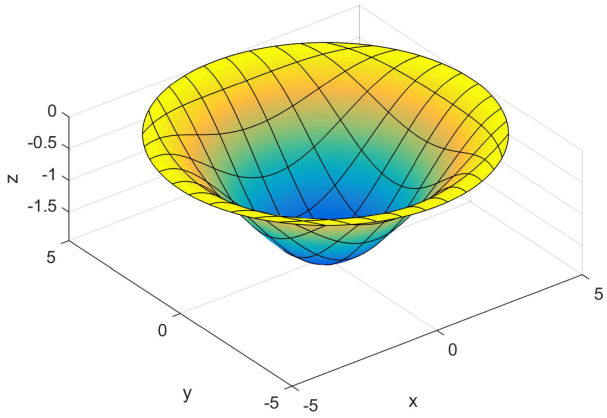

(a) $\bar{\omega}_1 = 7.3195$.

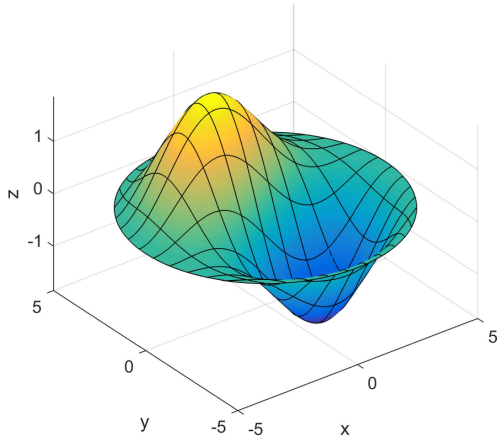

(b) $\bar{\omega}_2 = 14.0950$.

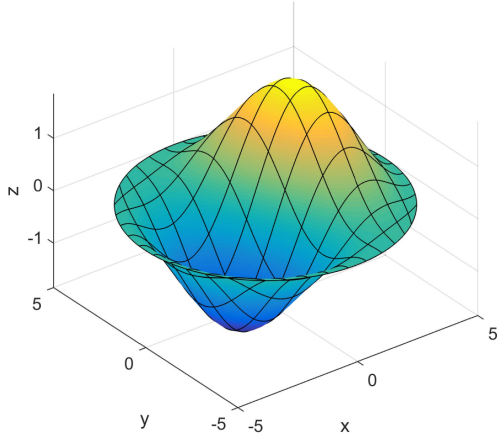

(c) $\bar{\omega}_3 = 14.0950$.

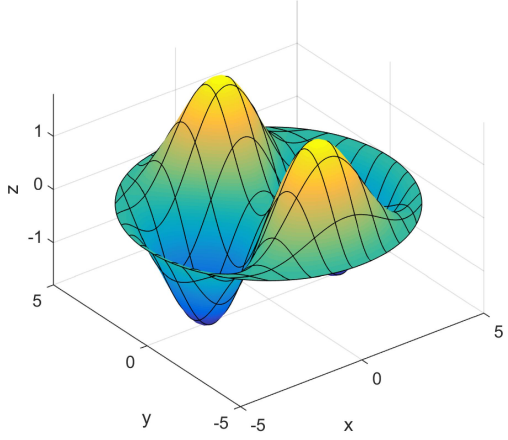

(d) $\bar{\omega}_4 = 21.3095$.

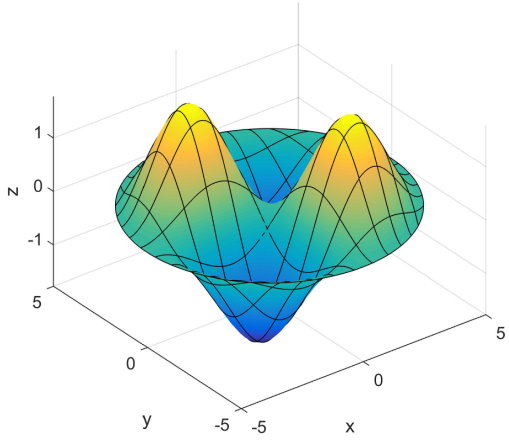

(e) $\bar{\omega}_5 = 21.7503$.

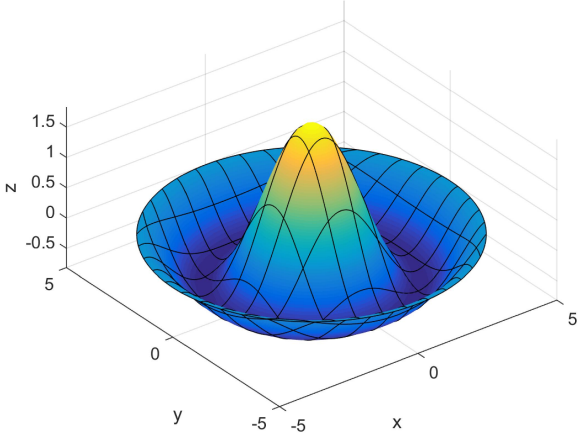

(f) $\bar{\omega}_6 = 23.9885$.

Figure 13: The first six free vibration mode shapes of clamped Al/Al_2O_3 circular microplates.

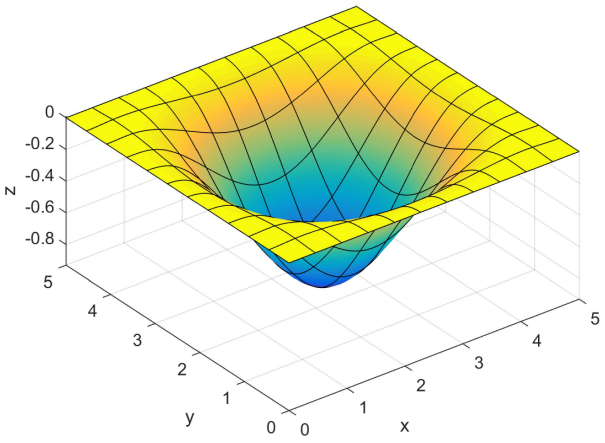

(a) $\bar{P}_1 = 52.1032$.

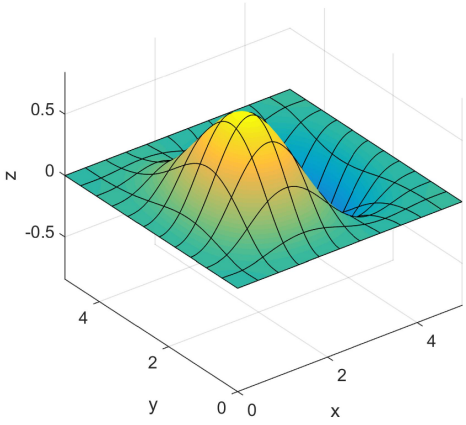

(b) $\bar{P}_2 = 66.3156$.

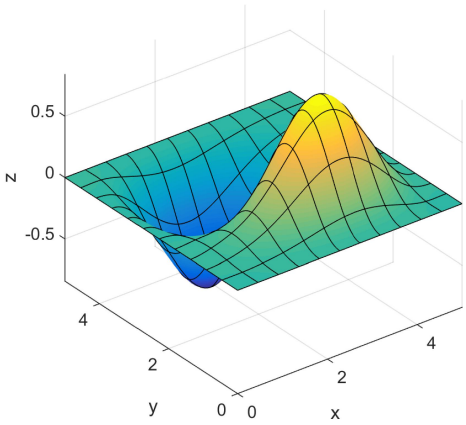

(c) $\bar{P}_3 = 66.3156$.

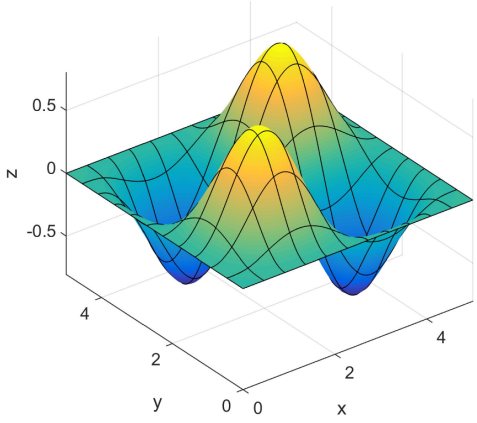

(d) $\bar{P}_4 = 77.2179$.

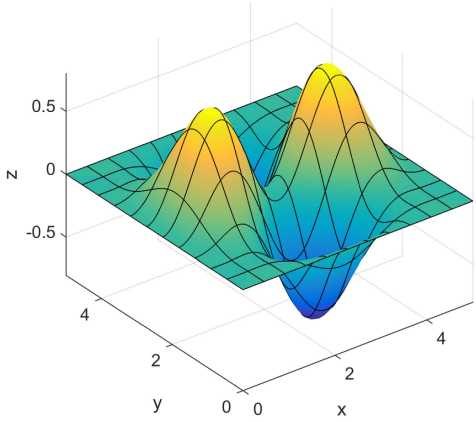

(e) $\bar{P}_5 = 78.9774$.

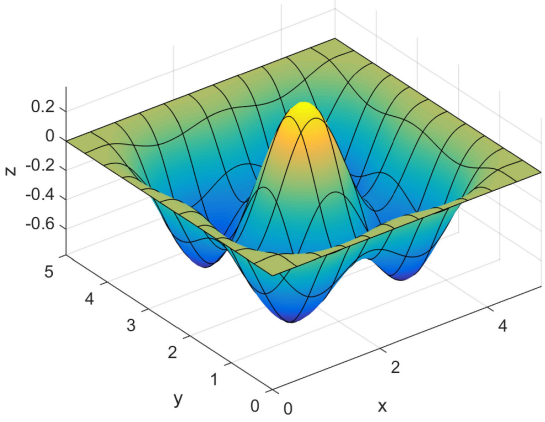

(f) $\bar{P}_6 = 84.1043$.

Figure 14: The first six buckling mode shapes of Al/Al_2O_3 CCCC square microplates.

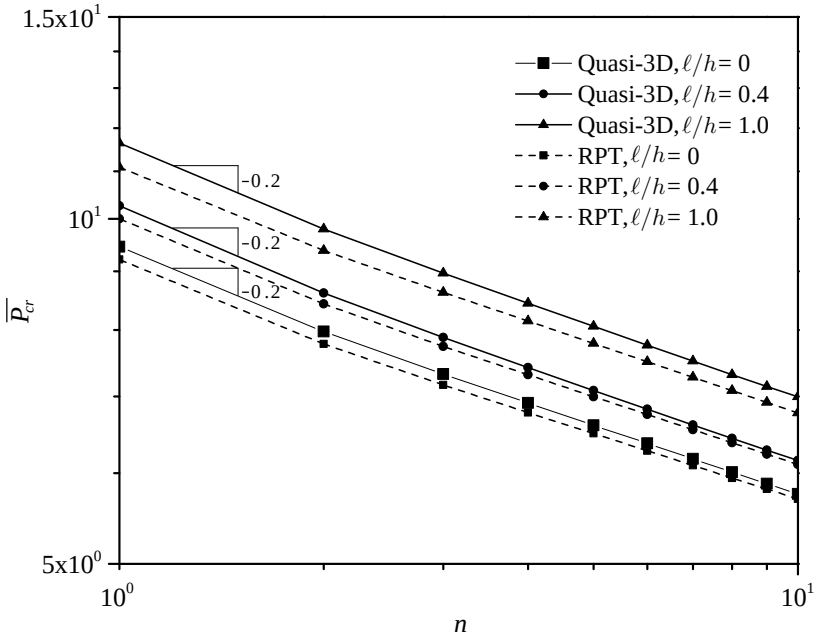

(a) Simply support.

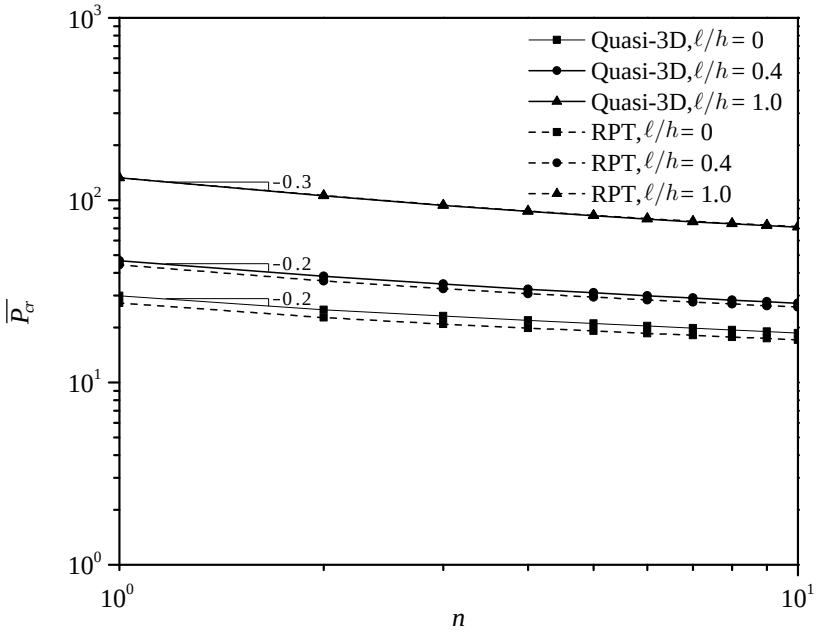

(b) Clamped support.

Figure 15: Effects of material index n and material length scale ratio ℓ/h on the critical buckling loads of Al/Al_2O_3 circular microplates, $h/R = 0.2$ (Mori-Tanaka scheme).

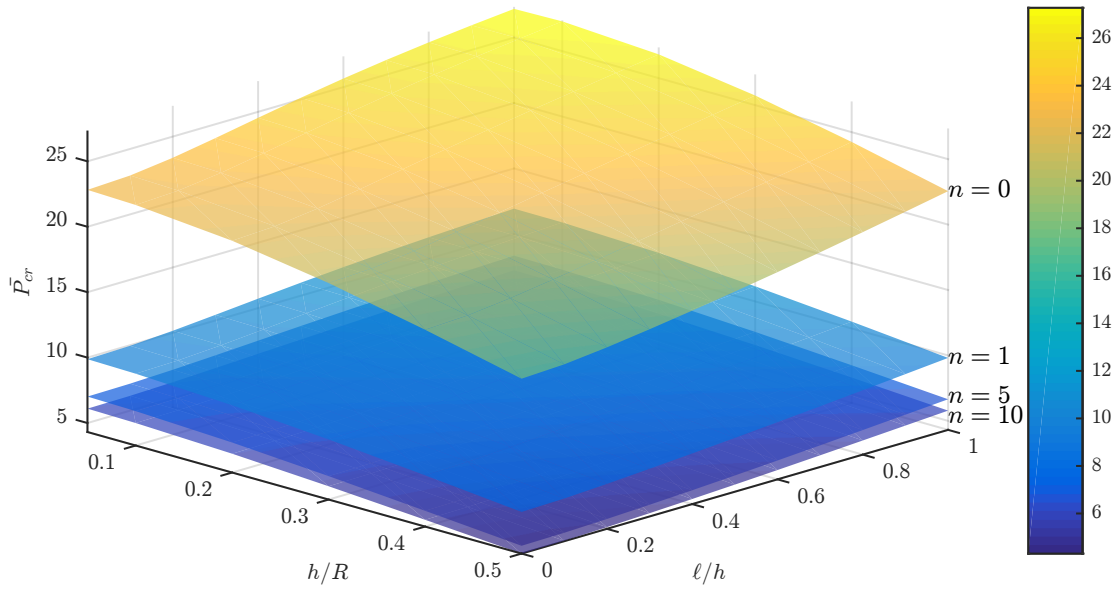

Figure 16: Variation of the critical buckling loads of Al/Al_2O_3 circular microplates (Mori-Tanaka scheme).

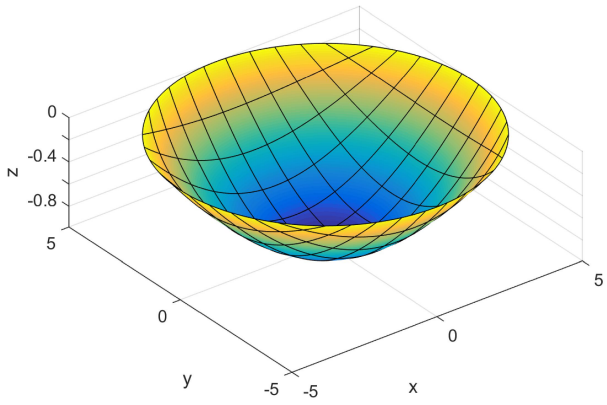

(a) $\bar{P}_1 = 10.7545$.

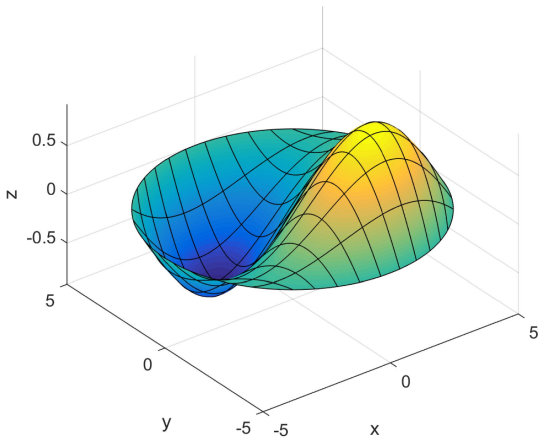

(b) $\bar{P}_2 = 49.5358$.

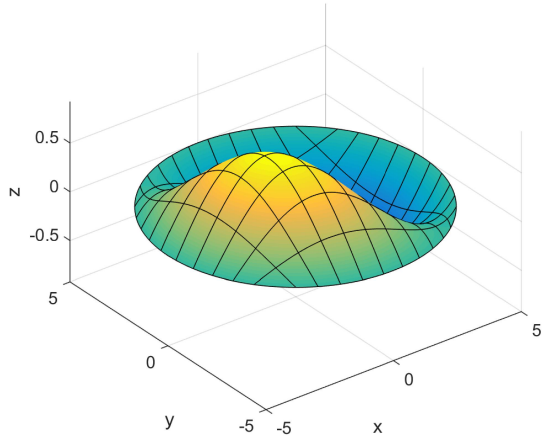

(c) $\bar{P}_3 = 49.5358$.

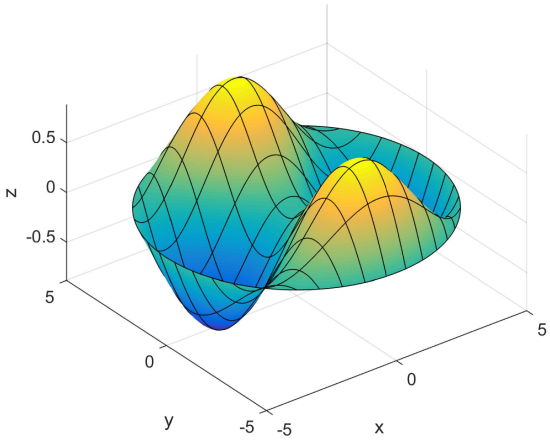

(d) $\bar{P}_4 = 80.6606$.

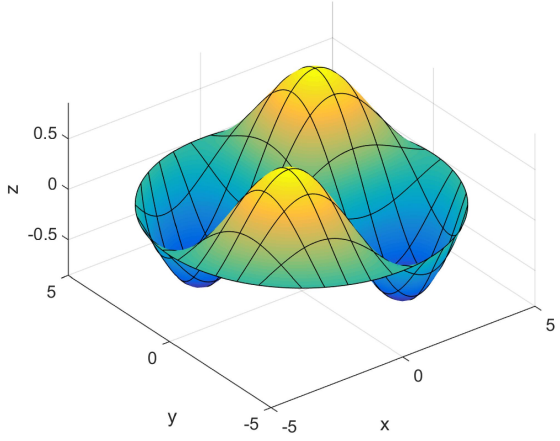

(e) $\bar{P}_5 = 104.8026$.

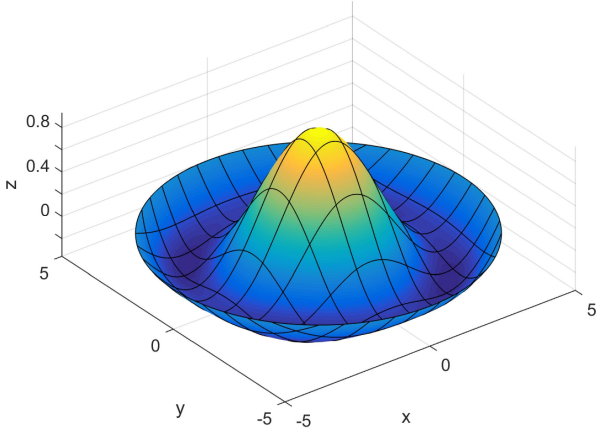

(f) $\bar{P}_6 = 108.1436$.

Figure 17: The first six buckling mode shapes of simply-supported Al/Al_2O_3 circular microplates.